Journal of Computational Physics 540 (2025) 114269

Contents lists available at ScienceDirect

Journal of Computational Physics

journal homepage: www.elsevier.com/locate/jcp

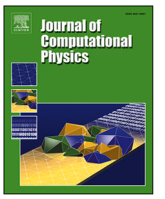

Physically consistent formulations of split convective terms for turbulent compressible multi-component flows

Ye Wang [a,*], Armin Wehrfritz [b], Evatt R. Hawkes [a]

[a] School of Mechanical and Manufacturing Engineering, The University of New South Wales, Sydney, Australia
[b] Department of Mechanical and Materials Engineering, University of Turku, Finland

ARTICLE INFO

Keywords:
Split convective forms
High-order finite-difference schemes
Compressible multi-component flows
Species mass fraction
Temperature equilibrium
Pressure equilibrium

ABSTRACT

We analyse the properties and characteristics of kinetic-energy-preserving, entropy-preserving, and pressure-equilibrium-preserving split convective forms for compressible multi-component flows. The results show that such schemes offer improved pressure-equilibrium-preserving properties and numerical stability compared to most other existing schemes, but also that the preservation of pressure equilibrium is not guaranteed for flows with varying specific heats. Furthermore, for the convective terms in species mass fraction transport equations, some split forms may fail to preserve key physical properties discretely. We construct a formulation for the species convective terms that consistently maintains these key physical properties, including species mass conservation, uniform mass fraction preservation, and temperature-equilibrium preservation. The capability of the proposed scheme in maintaining these properties is demonstrated analytically and tested in one-dimensional advection problems. Last, the proposed scheme is compared with schemes that do not satisfy these properties in under-resolved simulations of a modified inviscid Taylor–Green vortex flow. The results show improved performance of the proposed scheme and highlight the importance of a convective scheme for the species mass fractions to be able to consistently preserve these physical properties in a discrete sense.

1. Introduction

High-order and non-dissipative numerical schemes are advantageous for modelling compressible turbulence flows in direct numerical simulations and large-eddy simulations [1–4], due to their nature of small truncation errors [5,6] and low numerical diffusion [7] that enables high-fidelity turbulence simulations with reduced computational grid points. However, it is well known that such schemes lead to significant aliasing errors and may cause numerical instabilities [6,8], particularly for flows with high Reynolds numbers.

In high-Reynolds number turbulence simulations, aliasing errors arise when nonlinear convective terms (derivatives of multivariable products) are evaluated on a discrete grid, due to the under-resolved content above the Nyquist limit being misrepresented as (or aliased into) the resolved wavenumbers. Consequently, these errors often manifest as unphysical energy growth at higher wavenumbers, leading to inaccurate energy transfer and potential numerical instability [6,9]. In this situation, adding artificial dissipation such as high-order filters [10–12] becomes an option to remove the aliased energy and stabilise simulations; however, it is not always the first option [9]. As an alternative, recasting the convective terms in the 'skew-symmetric' split forms has been proposed to mitigate energy aliasing and nonlinear instability without needing artificial dissipation [6,9,13,14].

* Corresponding author.
E-mail addresses: ye.wang7@unswalumni.com (Y. Wang), armin.wehrfritz@utu.fi (A. Wehrfritz), evatt.hawkes@unsw.edu.au (E.R. Hawkes).

https://doi.org/10.1016/j.jcp.2025.114269
Received 25 June 2024; Received in revised form 29 July 2025; Accepted 1 August 2025
Available online 5 August 2025

Blaisdell et al. [13] showed that a quadratic-split form using spectral methods reduced these aliasing errors, compared to the divergence form. Kennedy and Gruber [9] further developed stable cubically split forms by fully expanding the triple products for flows with large density variations (e.g., compressible reacting flows), which showed lower aliasing errors and improved stability relative to quadratic-split forms. Unlike the analysis using exact Fourier modes by Blaisdell et al. [13] and Kennedy and Gruber [9], Kuya and Kawai [15] used the modified wavenumber of finite-difference operators to analyse the spectral characteristics of split forms. This analysis [15] showed that in finite-difference methods, the more stable split forms exhibited larger aliasing errors compared to the divergence form. This observation indicated that reducing aliasing errors of split forms may not always be the primary mechanism by which to improve stability in finite-difference methods [15], as also noted by Honein and Moin [16]. Furthermore, Honein and Moin [16] and Kuya and Kawai [15] suggested that preserving secondary conservative variables, such as kinetic energy and entropy, could be more crucial for improving numerical stability by the split forms in finite-difference methods.

Given the vital role of the kinetic energy balance in turbulence development, it is important that the numerical scheme is capable of representing the correct evolution of kinetic energy. As defined by Jameson [17], in kinetic-energy-preserving (KEP) schemes for compressible flows, the discrete volume integral of kinetic energy is not changed by the convective terms but only by the pressure work, ignoring the viscous terms, boundary conditions, and time integration errors. A KEP scheme can be easily obtained from the consistency condition due to Jameson [17], which was derived for second-order finite-volume schemes. KEP schemes have been successfully used in incompressible [18] and compressible simulations [2,19,20] to suppress numerical instabilities. Feiereisen et al. [19] proposed a quadratic-split form that is KEP for compressible flows. Pirozzoli [2] found a cubic-split form from Kennedy and Gruber [9] is also KEP, which has subsequently been applied in other studies [21,22]. Comparisons, such as those by Kuya et al. [22] and Gassner et al. [4], have indicated that this cubic-split form [2,9] was a promising approach for compressible flows regarding numerical robustness and computational efficiency. Other notable KEP schemes for compressible flows are based on square-root density splittings, such as the formulations of Morinishi [1] and Rozema et al. [23], and recent works [24,25].

Despite its success, discrete conservation of kinetic energy is not a sufficient condition for numerical stability in under-resolved simulations of compressible flows, and additional conditions such as entropy preservation have been proposed [26]. It has been shown that for schemes achieving discrete conservation of entropy[1], thermodynamic fluctuations converge and numerical instabilities are suppressed for high Reynolds number flows [16,21,22]. Following the concept by Tadmor [27], Chandrashekar [28] used the physical entropy as the mathematical entropy function to derive a second-order entropy-conservative scheme that is also KEP. However, Gassner et al. [4] reported its failure to preserve kinetic energy in a discontinuous Galerkin framework, which, due to the summation-by-parts property, shares many features with the finite-difference formulation. Ranocha [29] furthermore constructed an improved scheme that is entropy-conservative according to Tadmor's concept and preserves kinetic energy. A different approach was taken by Honein and Moin [16], who enforced exact conservation of the physical entropy by solving a modified internal energy equation that is numerically equivalent to the entropy equation. Similarly, Coppola et al. [21] achieved exact entropy conservation by directly solving the entropy equation. Interestingly, they also found that solving the standard internal energy equation in the cubic-split form nearly conserves entropy. Although a rigorous proof was not offered by Coppola et al. [21], this outcome may be linked to implicit entropy conservation via the Gibbs equation, which, as described by Subbareddy and Candler [20] and Kuya et al. [22], relates the continuity and internal energy equations with the entropy equation. Based on the Gibbs equation, consistency conditions were summarised in Refs. [3,22,30]; satisfying these conditions helps correctly represent local energy exchange between kinetic energy and internal energy, and thus supports entropy conservation. Particularly, the kinetic-energy- and entropy-preserving (KEEP) scheme due to Kuya et al. [22] achieved discrete entropy conservation implicitly by solving the total energy equation with consistent split-form numerical fluxes. This approach is preferred as it also conserves total energy, which is important for compressible problems. Although this method does not conserve entropy exactly, the entropy conservation errors were small [22,30,31] and adjustable [32].

However, subsequent research by Shima et al. [31] found that despite conserving kinetic energy, entropy, and total energy, the split form by Kuya et al. [22] led to numerical instability in a resolved single-component flow with initially uniform pressure and velocity but varying density. This instability was attributed to spurious pressure oscillations induced by the cubic-split form for internal energy. To remedy this, Shima et al. [31] suggested a quadratic-split form that eliminated these oscillations, thus preserving pressure equilibrium and stabilising the simulation with a slight impact on entropy conservation. They described pressure equilibrium in inviscid, ideal-gas, single-component flows as the physical property where initially uniform pressure and velocity remain constant despite variations in density, and characterised their scheme, which consistently maintains this property in the discrete level, as pressure-equilibrium-preserving (PEP). Ranocha and Gassner [33] subsequently found the entropy-conservative and KEP scheme developed by Ranocha [29] is also PEP. However, this scheme has stability issues due to the use of logarithmic means in the density flux [33] and is computationally expensive. Additionally, De Michele and Coppola recently confirmed the square-root splitting proposed by Rozema et al. [23] to be PEP [34] and to exhibit excellent entropy conservation [35], as further explored by Kawai and Kawai [36]. De Michele and Coppola [34] also constructed new PEP schemes through minor modifications to classical numerical fluxes of Pirozzoli [2] and Kuya et al. [22]. These modifications were shown to improve the overall performance of the original schemes without

[1] Entropy in this article refers to the physical entropy, unless stated otherwise. Entropy conservation means that the discrete volume integral of the physical entropy is not changed by the convective terms and is preserved over time, assuming the viscous terms, boundary conditions and time integration errors are ignored.

increasing computational cost in ideal-gas, single-component flows. On the other hand, in multi-component flows, ensuring pressure equilibrium across interfaces, where jumps in specific heats may occur, presents extra challenges, particularly within a fully conservative system [37,38]. Despite many studies working on this issue [39–41], the application of split forms for maintaining pressure equilibrium had not been explored until the recent work by Fujiwara et al. [42]. They proposed a fully conservative split-form scheme that preserves pressure equilibrium at interfaces without jumps for calorically perfect gases, which reduces to the scheme by Shima et al. [31] for uniform concentrations. The entropy-conservative schemes in Tadmor's framework (e.g., Ranocha [29]) have also recently been extended to multi-component, thermally perfect gas in a discontinuous Galerkin setting [43,44]. However, these do not satisfy a strict PEP property. Furthermore, Jain and Moin [30] derived a condition to preserve pressure equilibrium at two-phase flow interfaces, which requires identical split forms for internal energy and total mass, resulting in the same split forms as Shima et al. [31]. While different split forms were evaluated by Jain and Moin [30], a uniform specific heat ratio was assumed. In other related studies, more sophisticated PEP split forms have been constructed for real-fluid simulations to address challenges arising from highly nonlinear relations between pressure and internal energy [45,46]. Therefore, although various split forms of PEP schemes have been proposed over the past few years, discussion on most schemes in multi-component, compressible flows with varying specific heats remains limited. In particular, there is no thorough evaluation of the PEP schemes by Shima et al. [31] and Rozema et al. [23] in this context, leaving open questions about whether they still outperform other split forms, such as those that only preserve kinetic energy [2] or entropy [22], and how they compare to PEP schemes specifically designed for multi-component flows, such as the one by Fujiwara et al. [42].

For multi-component flows, the numerical schemes for the convective terms in the species mass transport equations require further careful consideration. The discrete conservation of species mass should first be preserved. This is particularly important in chemically reacting flows as a prerequisite for accurately evaluating reaction rates and other properties. When solving conservative species equations, Trisjono et al. [47] suggested discretely satisfying the advection forms of these equations, as it helps avoid an initially uniform species field being disturbed spuriously for flows with non-uniform density or velocity. Additionally, Terashima et al. [41] noted that properly treating the molar concentration, associated with species partial densities, is important to preserve temperature equilibrium at material interfaces. Although this challenge is typically encountered at material interfaces of multi-component flows [40,41], we will show that even with uniform specific heats and preserved pressure equilibrium, improper reconstructions of partial densities at flux points can cause spurious temperature oscillations. This was also discussed by Subbareddy et al. [48] for finite-volume methods. They advised against separating total density and species mass fraction when reconstructing partial densities at cell faces to prevent large temperature excursions. Otherwise, for systems solving equations for all species without the continuity equation, numerical schemes need to ensure that all partial densities sum to the mixture density [48]. Jain and Moin [30] implemented this condition in constructing split-form numerical fluxes for phase masses in multiphase flows. Nevertheless, very few studies have explored split forms for the convective terms in species mass transport equations, and to the best of our knowledge, the characteristics of different split forms for species convective terms have not been discussed, particularly regarding the key physical properties discussed above, including species mass conservation, uniform species field and temperature-equilibrium preservation. This gap remains despite the fact that some studies have applied split forms to species convective terms. For instance, Kennedy and Gruber [9] adopted split forms with better aliasing behaviour and computational efficiency, Pantano et al. [49] used a quadratic-split form to improve stability, Fujiwara et al. [42] employed a quadratic-split form for its compatibility with their pressure-equilibrium condition, and Terashima et al. [46] also chose a quadratic-split form when constructing their approximate PEP scheme. While Fujiwara et al. [42] discussed the PEP property of their quadratic-split form and a divergence form, their characteristics concerning the key physical properties mentioned above were not explored.

Therefore, the focus in the present study is on the development of a high-order, non-dissipative, accurate, stable and physically consistent[2] finite-difference scheme for turbulent compressible multi-component flows. The first objective is to evaluate the performance and properties of schemes using the pressure-equilibrium-preserving split forms, including the schemes by Shima et al. [31] and Rozema et al. [23], in the context of multi-component flows. This evaluation includes a comparison with other existing schemes such as low-aliasing, kinetic-energy-preserving, or entropy-preserving schemes, and with the multi-component pressure-equilibrium-preserving scheme by Fujiwara et al. [42]. The properties of the schemes are investigated by analytical methods and their performance is tested in numerical experiments. A second objective is to construct a scheme for convective terms in the species mass transport equations based on the essential physical properties, including species mass conservation, uniform species field and temperature-equilibrium preservation. The capability of the proposed scheme in maintaining these physical properties is demonstrated analytically and verified in numerical tests. It is also compared to other possible schemes that do not satisfy these physical properties, to highlight the importance of using physically consistent forms in computing the mass fraction and temperature. It should be noted that we specifically aim at constructing high-order schemes for direct numerical simulations, and thus all formulations are derived for an arbitrary order of accuracy, and all numerical tests are carried out using eighth-order schemes.

The remainder of this article is organised as follows. Section 2 summarises the governing equations. Section 3 describes the conditions and formulations for the schemes which are in the numerical flux form, along with a summary of the schemes to be tested. Section 4 presents the numerical tests in terms of the two objectives, followed by concluding remarks in Section 5.

[2] We say a scheme is physically consistent if the scheme consistently maintains relevant physical properties discretely.

2. Governing equations

2.1. Conservation equations

We are interested in solving the compressible, multi-component, chemically-reacting flow equations. However, given the current focus on numerical schemes for the convective terms, we consider the inviscid system, which contains the classical three-dimensional, compressible Euler equations for the mixture and additional species transport equations, as widely considered in the community [9,40,49–53]:

$$\frac{\partial \rho}{\partial t} + \frac{\partial \rho u_j}{\partial x_j} = 0, \tag{1}$$

$$\frac{\partial \rho u_i}{\partial t} + \frac{\partial \rho u_i u_j}{\partial x_j} + \frac{\partial p}{\partial x_i} = 0, \tag{2}$$

$$\frac{\partial \rho E}{\partial t} + \frac{\partial \rho E u_j}{\partial x_j} + \frac{\partial p u_j}{\partial x_j} = 0, \tag{3}$$

$$\frac{\partial \rho Y_\alpha}{\partial t} + \frac{\partial \rho Y_\alpha u_j}{\partial x_j} = 0, \ \alpha = 1, \cdots, N_s - 1, \tag{4}$$

where t denotes time, x_i are the spatial coordinates in a Cartesian coordinate system, u_i is the velocity vector component in the i^{th} direction, ρ is the mixture density, p is the mixture total pressure, Y_α is the mass fraction of species α, and N_s is the total number of species. Only $N_s - 1$ species equations are solved and the mass fraction of species N_s is determined from the constraint: $\sum_{\alpha=1}^{N_s} Y_\alpha = 1$. This approach ensures that the mass fractions of all species sum up to unity by design. The specific total energy, $E = e + k$, is the sum of mixture specific internal energy, e, and specific kinetic energy, $k = u_i u_i/2$. Accordingly, as in Kuya et al. [22], we can rewrite the total energy equation (Eq. (3)) as

$$\frac{\partial \rho E}{\partial t} + \frac{\partial \rho e u_j}{\partial x_j} + \frac{\partial \rho k u_j}{\partial x_j} + \frac{\partial p u_j}{\partial x_j} = 0. \tag{5}$$

Similarly, as in Pirozzoli [2], using the mixture total specific enthalpy, $H = E + p/\rho$, the total energy equation (Eq. (3)) becomes:

$$\frac{\partial \rho E}{\partial t} + \frac{\partial \rho H u_j}{\partial x_j} = 0. \tag{6}$$

In the discussed equations, the conserved variables are solved directly, and the convective terms are expressed in the divergence form. This approach is commonly used in compressible solvers [52,54] to discretely conserve total mass, momentum, total energy, and species mass. However, as will be explored in Section 3, there are alternative convective formulations that are analytically equivalent to the divergence form. Despite being numerically different, these formulations may also achieve similar discrete conservation.

2.2. Equation of state

We assume that the species are calorically perfect gases in thermal equilibrium, each with constant specific heat capacities $C_{p,\alpha}$ and $C_{v,\alpha}$. Consequently, the mean specific heats of their mixture alter with composition but remain constant with temperature changes. This simplifies the computation of thermodynamic relations by using mixing rules. It also allows for diverse spatial distributions of the mixture specific heats, a critical aspect of our study on pressure equilibrium in multi-component flows. The specific internal energy of species α is

$$e_\alpha = C_{v,\alpha} T = \frac{R_u/W_\alpha}{\gamma_\alpha - 1} T = \frac{p_\alpha}{\rho_\alpha(\gamma_\alpha - 1)}, \tag{7}$$

and the mixture specific internal energy is given by

$$e = \sum_{\alpha=1}^{N_s} Y_\alpha e_\alpha. \tag{8}$$

Therein, T is the temperature, R_u is the universal gas constant, W_α and γ_α are respectively the molar mass and the specific heat ratio of species α, the partial pressure is $p_\alpha = pX_\alpha$ with X_α denoting the species mole fraction, and the partial density $\rho_\alpha = \rho Y_\alpha$ denotes the density of species α. With the relation $Y_\alpha/X_\alpha = W_\alpha/W$, the mean molar mass of the mixture, W, is

$$W = \sum_{\alpha=1}^{N_s} X_\alpha W_\alpha = \left(\sum_{\alpha=1}^{N_s} \frac{Y_\alpha}{W_\alpha} \right)^{-1}. \tag{9}$$

The mean specific heat ratio of the mixture is $\gamma = C_p/C_v$, where $C_p = \sum_{\alpha=1}^{N_s} Y_\alpha C_{p,\alpha}$ and $C_v = \sum_{\alpha=1}^{N_s} Y_\alpha C_{v,\alpha}$ are the mean specific heats, and γ can be obtained from:

$$\frac{1}{\gamma - 1} = \sum_{\alpha=1}^{N_s} \frac{X_\alpha}{\gamma_\alpha - 1}. \tag{10}$$

Then, we obtain the thermodynamic equation of state for the mixture:

$$e = \frac{p}{\rho(\gamma - 1)}, \tag{11}$$

which closes the balance equations, and the mixture ideal-gas law:

$$p = \rho \frac{R_u}{W} T. \tag{12}$$

3. Numerical flux form of split convective terms

3.1. Numerical flux form

For compressible flows that may develop discontinuities, it is beneficial to globally conserve the primary invariants (i.e., total mass, momentum, total energy, and species mass) in a discrete sense, since according to the Lax–Wendroff theorem [55], it assures the discrete solution converges to a unique weak solution upon grid convergence. The numerical flux form, which casts the discretisation of convective terms in the difference of numerical fluxes at adjacent intermediate nodes, ensures global conservation through the telescopic property [55]. It is also known as the local conservative form [14], and it achieves better numerical stability than forms without discrete conservation [21]. Using F to represent a generic flux function, the spatial derivative in the j^{th} direction at grid point m is discretised using the numerical flux form:

$$\left.\frac{\partial F_j}{\partial x_j}\right|_m \approx \frac{\hat{F}_j|_{m+\frac{1}{2}} - \hat{F}_j|_{m-\frac{1}{2}}}{\Delta x_j}, \tag{13}$$

where $\hat{F}_j|_{m\pm\frac{1}{2}}$ denotes the numerical flux at the flux point $m \pm \frac{1}{2}$ between grid points m and $m \pm 1$, and Δx_j is the grid spacing size.

Applying the generic numerical flux (Eq. (13)), the semi-discrete representation for Eqs. (1)–(4) can be expressed as:

$$\left.\frac{\partial \rho}{\partial t}\right|_m + \frac{\hat{C}_j|_{m+\frac{1}{2}} - \hat{C}_j|_{m-\frac{1}{2}}}{\Delta x_j} = 0, \tag{14}$$

$$\left.\frac{\partial \rho u_i}{\partial t}\right|_m + \frac{\hat{M}_{ij}|_{m+\frac{1}{2}} - \hat{M}_{ij}|_{m-\frac{1}{2}}}{\Delta x_j} + \frac{\hat{G}|_{m+\frac{1}{2}} - \hat{G}|_{m-\frac{1}{2}}}{\Delta x_i} = 0, \tag{15}$$

$$\left.\frac{\partial \rho E}{\partial t}\right|_m + \frac{\hat{E}_j|_{m+\frac{1}{2}} - \hat{E}_j|_{m-\frac{1}{2}}}{\Delta x_j} + \frac{\hat{D}_j|_{m+\frac{1}{2}} - \hat{D}_j|_{m-\frac{1}{2}}}{\Delta x_j} = 0, \tag{16}$$

$$\left.\frac{\partial \rho Y_\alpha}{\partial t}\right|_m + \frac{\hat{Y}_{\alpha,j}|_{m+\frac{1}{2}} - \hat{Y}_{\alpha,j}|_{m-\frac{1}{2}}}{\Delta x_j} = 0,\ \alpha = 1, \cdots, N_s - 1, \tag{17}$$

where $\hat{C}_j$, $\hat{M}_{ij}$, $\hat{G}$, $\hat{E}_j$, $\hat{D}_j$, and $\hat{Y}_{\alpha,j}$ are the total mass, momentum (in the i^{th} direction), pressure-gradient, total energy, pressure-diffusion, and species mass (for species α) numerical fluxes, respectively. Many compressible flow solvers (e.g., [52]) adopt the intuitive formulation of the energy equation (Eq. (16)), which was also used by Kennedy and Gruber [9]. An alternative formulation, based on separating the internal and kinetic energy (Eq. (18)), was used by Kok [3], Kuya et al. [22], Shima et al. [31], and Jain and Moin [30], whereas Jameson [17] and Pirozzoli [2] used the total enthalpy leading to Eq. (19):

$$\left.\frac{\partial \rho E}{\partial t}\right|_m + \frac{\hat{I}_j|_{m+\frac{1}{2}} - \hat{I}_j|_{m-\frac{1}{2}}}{\Delta x_j} + \frac{\hat{K}_j|_{m+\frac{1}{2}} - \hat{K}_j|_{m-\frac{1}{2}}}{\Delta x_j} + \frac{\hat{D}_j|_{m+\frac{1}{2}} - \hat{D}_j|_{m-\frac{1}{2}}}{\Delta x_j} = 0, \tag{18}$$

$$\left.\frac{\partial \rho E}{\partial t}\right|_m + \frac{\hat{H}_j|_{m+\frac{1}{2}} - \hat{H}_j|_{m-\frac{1}{2}}}{\Delta x_j} = 0, \tag{19}$$

where $\hat{I}_j$, $\hat{K}_j$, and $\hat{H}_j$ are the internal energy, kinetic energy, and total enthalpy numerical fluxes, respectively. Coppola et al. [21] employed the internal energy equation:

$$\left.\frac{\partial \rho e}{\partial t}\right|_m + \frac{\hat{I}_j|_{m+\frac{1}{2}} - \hat{I}_j|_{m-\frac{1}{2}}}{\Delta x_j} + p|_m \frac{\hat{U}_j|_{m+\frac{1}{2}} - \hat{U}_j|_{m-\frac{1}{2}}}{\Delta x_j} = 0, \tag{20}$$

where $\hat{U}_j$ is the numerical flux for $\partial u_j/\partial x_j$ in the pressure-dilation term ($p\partial u_j/\partial x_j$).

3.2. 'Skew-symmetric' split form

To simplify the notation, we will introduce the split forms in one dimension. The extension to two and three dimensions is trivial. The generic flux function can be expressed as $F = fg$ and $F = fgh$ respectively for quadratically and cubically nonlinear derivatives, where f, g, and h are arbitrary functions of x. Quadratically nonlinear derivatives can be split as:

$$\frac{\partial fg}{\partial x} = \alpha_q \frac{\partial fg}{\partial x} + (1 - \alpha_q)\left(f\frac{\partial g}{\partial x} + g\frac{\partial f}{\partial x}\right), \tag{21}$$

where α_q is an arbitrary coefficient. Ducros et al. [14] first showed that this split form with $\alpha_q = 1/2$ can be written in the numerical flux form for explicit central-difference approximations. Fisher et al. [56] proved that the telescopic property [55] is satisfied for any constant α_q in conservation law equations discretised using any diagonal-norm split summation-by-part (SBP) operators. For cubically nonlinear derivatives, Kennedy and Gruber [9] derived the general split form:

$$\frac{\partial fgh}{\partial x} = \alpha_c \frac{\partial fgh}{\partial x} + \beta\left(f\frac{\partial gh}{\partial x} + gh\frac{\partial f}{\partial x}\right) + \kappa\left(g\frac{\partial fh}{\partial x} + fh\frac{\partial g}{\partial x}\right) + \delta\left(h\frac{\partial fg}{\partial x} + fg\frac{\partial h}{\partial x}\right) + \zeta\left(gh\frac{\partial f}{\partial x} + fh\frac{\partial g}{\partial x} + fg\frac{\partial h}{\partial x}\right), \tag{22}$$

where $\alpha_c + \beta + \kappa + \delta + \zeta = 1$. Eq. (22) contains all the possible combinations in Eq. (21) by letting the function $h = 1$, the coefficients $\alpha_c + \delta = \alpha_q$, and $\beta + \kappa = 1 - \alpha_q$. However, not all combinations of Eq. (22) can be cast into the numerical flux form (Eq. (13)) [2,21], such as the formulation with $\alpha_c = \zeta = \frac{1}{2}$ and $\beta = \kappa = \delta = 0$, referred to here as the KG form:

$$\frac{\partial fgh}{\partial x} = \frac{1}{2}\frac{\partial fgh}{\partial x} + \frac{1}{2}\left(gh\frac{\partial f}{\partial x} + fh\frac{\partial g}{\partial x} + fg\frac{\partial h}{\partial x}\right). \tag{23}$$

The KG form (Eq. (23)) demonstrates low aliasing errors and good numerical stability, as tested by Kennedy and Gruber [9], despite lacking conservation of primary quantities (except for total mass) and secondary quantities (kinetic energy and entropy). We include the KG form (Eq. (23)) in this study for comparative evaluation with the schemes introduced later in Section 3.3. For compressible multi-component flows, the governing equations split using the KG form read:

$$\frac{\partial \rho}{\partial t} + \frac{1}{2}\frac{\partial \rho u_j}{\partial x} + \frac{1}{2}\left(u_j\frac{\partial \rho}{\partial x} + \rho\frac{\partial u_j}{\partial x}\right) = 0, \tag{24}$$

$$\frac{\partial \rho u_i}{\partial t} + \frac{1}{2}\frac{\partial \rho u_i u_j}{\partial x} + \frac{1}{2}\left(u_i u_j\frac{\partial \rho}{\partial x} + \rho u_j\frac{\partial u_i}{\partial x} + \rho u_i\frac{\partial u_j}{\partial x}\right) + \frac{\partial p}{\partial x_i} = 0, \tag{25}$$

$$\frac{\partial \rho E}{\partial t} + \frac{1}{2}\frac{\partial \rho E u_j}{\partial x} + \frac{1}{2}\left(Eu_j\frac{\partial \rho}{\partial x} + \rho u_j\frac{\partial E}{\partial x} + \rho E\frac{\partial u_j}{\partial x}\right) + \frac{1}{2}\frac{\partial p u_j}{\partial x} + \frac{1}{2}\left(u_j\frac{\partial p}{\partial x} + p\frac{\partial u_j}{\partial x}\right) = 0, \tag{26}$$

$$\frac{\partial \rho Y_\alpha}{\partial t} + \frac{1}{2}\frac{\partial \rho Y_\alpha u_j}{\partial x} + \frac{1}{2}\left(Y_\alpha u_j\frac{\partial \rho}{\partial x} + \rho u_j\frac{\partial Y_\alpha}{\partial x} + \rho Y_\alpha\frac{\partial u_j}{\partial x}\right) = 0,\ \alpha = 1, \cdots, N_s - 1. \tag{27}$$

On the other hand, Coppola et al. [21] showed that $\zeta = 0$ is a sufficient condition for casting Eq. (22) into numerical flux form for explicit central-difference approximations, assuming all the coefficients are constants. With this constraint, we obtain four formulations:

$$\text{Divergence form}: \frac{\partial fgh}{\partial x}, \tag{28}$$

$$\text{Quadratic-split form}: \frac{1}{2}\left(\frac{\partial fgh}{\partial x} + f\frac{\partial gh}{\partial x} + gh\frac{\partial f}{\partial x}\right), \tag{29}$$

$$\text{Cubic-split form}: \frac{1}{4}\left(\frac{\partial fgh}{\partial x} + f\frac{\partial gh}{\partial x} + gh\frac{\partial f}{\partial x} + g\frac{\partial fh}{\partial x} + fh\frac{\partial g}{\partial x} + h\frac{\partial fg}{\partial x} + fg\frac{\partial h}{\partial x}\right), \tag{30}$$

$$\text{Product-rule form}: f\frac{\partial gh}{\partial x} + gh\frac{\partial f}{\partial x}, \tag{31}$$

where the terminology extends to the quadratically nonlinear derivatives by setting $h = 1$. The quadratic-split ($\alpha_c = \beta = \frac{1}{2}; \kappa = \delta = \zeta = 0$) and cubic-split ($\alpha_c = \beta = \kappa = \delta = \frac{1}{4}; \zeta = 0$) forms are referred to as the 'standard' split forms by Pirozzoli [2] and are widely used [4,22,30]. Additionally, we consider the square-root-based split form due to Rozema et al. [23] (see also De Michele and Coppola [34] and Kawai and Kawai [36]):

$$\text{Square-root form}: \frac{1}{2}\left(\sqrt{g}\frac{\partial f\sqrt{g}h}{\partial x} + f\sqrt{g}h\frac{\partial \sqrt{g}}{\partial x}\right) + \frac{1}{2}\left(f\sqrt{g}\frac{\partial \sqrt{g}h}{\partial x} + \sqrt{g}h\frac{\partial f\sqrt{g}}{\partial x}\right). \tag{32}$$

Note that varying combinations of f, g, and h may result in different discretisation schemes, each with different properties. For instance, the quadratic-split form by Feiereisen et al. [19] using $f = u_i$, $g = \rho$, and $h = u_j$ is KEP, whereas the one due to Blaisdell et al. [13] with $f = u_j$, $g = \rho$, and $h = u_i$ is not.

Applying the two-point discrete averaging operator from Pirozzoli [2] and Coppola et al. [21], and invoking the generic numerical flux (Eq. (13)), the numerical fluxes for these split forms in the $2L^{\text{th}}$-order accuracy are expressed as:

$$\hat{F}|_{m+\frac{1}{2}} = 2\sum_{l=1}^{L} a_{L,l} \sum_{k=0}^{l-1} (\widetilde{f,g,h})_{m-k,l}, \tag{33}$$

where $a_{L,l}$ is the coefficients in the standard explicit central-difference approximation of the first-order derivative with the formal order of accuracy of $2L$, and $(\widetilde{f,g,h})_{m-k,l}$ is the two-point discrete averaging operator. The corresponding operators to the forms in Eqs. (28)–(32) are:

$$(\widetilde{f,g,h})^{\text{Divergence}}_{m-k,l} = \frac{(fgh)|_{m-k} + (fgh)|_{m-k+l}}{2}, \tag{34}$$

$$(\widetilde{f,g,h})^{\text{Quadratic-split}}_{m-k,l} = \frac{f|_{m-k} + f|_{m-k+l}}{2}\frac{(gh)|_{m-k} + (gh)|_{m-k+l}}{2}, \tag{35}$$

$$(\widetilde{f,g,h})^{\text{Cubic-split}}_{m-k,l} = \frac{f|_{m-k}+f|_{m-k+l}}{2}\frac{g|_{m-k}+g|_{m-k+l}}{2}\frac{h|_{m-k}+h|_{m-k+l}}{2}, \tag{36}$$

$$(\widetilde{f,g,h})^{\text{Product-rule}}_{m-k,l} = \frac{f|_{m-k+l}(gh)|_{m-k}+f|_{m-k}(gh)|_{m-k+l}}{2}, \tag{37}$$

$$(\widetilde{f,g,h})^{\text{Square-root}}_{m-k,l} = \frac{f|_{m-k}+f|_{m-k+l}}{2}\sqrt{g|_{m-k}g|_{m-k+l}}\frac{h|_{m-k}+h|_{m-k+l}}{2}. \tag{38}$$

All numerical fluxes in this study, except for the kinetic energy numerical flux, can be derived by substituting f, g, and h with corresponding flow variables. Note that although we focus only on standard explicit schemes in this study, the split forms may also be discretised with compact stencils [57,58].

3.3. Consistent forms for compressible multi-component flows

3.3.1. Total mass and momentum numerical fluxes

The numerical fluxes for total mass, $\hat{C}_j$, and momentum, $\hat{M}_{ij}$, are required to satisfy the kinetic-energy-preserving (KEP) property discretely. Jameson [17] derived a KEP condition:

$$\hat{M}_j|_{m+\frac{1}{2}} = \hat{C}_j|_{m+\frac{1}{2}}\frac{u_i|_m+u_i|_{m+1}}{2}, \tag{39}$$

satisfying which results in a group of KEP schemes. However, this condition is confined to second-order accuracy and does not explicitly extend to high-order numerical fluxes. In Theorem 1, we extend the KEP condition to numerical fluxes in an arbitrary order of accuracy, with a proof provided in Appendix A.

Theorem 1. *In the semi-discrete sense, the total kinetic energy is globally conserved, i.e., it is not changed by the convective terms but only changed by the pressure work and boundary terms, if the numerical fluxes in $2L^{th}$-order accuracy for total mass,*

$$\hat{C}_j|_{m+\frac{1}{2}} = 2\sum_{l=1}^{L} a_{L,l}\sum_{k=0}^{l-1}(\widetilde{\rho,u_j,1})_{m-k,l}, \tag{40}$$

and momentum,

$$\hat{M}_j|_{m+\frac{1}{2}} = 2\sum_{l=1}^{L} a_{L,l}\sum_{k=0}^{l-1}(\widetilde{\rho,u_j,u_i})_{m-k,l}, \tag{41}$$

satisfy the condition:

$$(\widetilde{\rho,u_j,u_i})_{m-k,l} = (\widetilde{\rho,u_j,1})_{m-k,l}\frac{u_i|_{m-k}+u_i|_{m-k+l}}{2}, \tag{42}$$

where the two-point discrete averaging operators, $\widetilde{(\cdot,\cdot,\cdot)}$, are defined in Eqs. (34)–(38).

Proof. Appendix A. □

According to this condition, we can formulate KEP numerical fluxes with arbitrary order of accuracy. For instance, the standard quadratic-split and cubic-split forms are represented by

$$\hat{C}_j|_{m+\frac{1}{2}} = 2\sum_{l=1}^{L} a_{L,l}\sum_{k=0}^{l-1}\frac{\rho|_{m-k}+\rho|_{m-k+l}}{2}\frac{u_j|_{m-k}+u_j|_{m-k+l}}{2}, \tag{43}$$

$$\hat{M}_{ij}|_{m+\frac{1}{2}} = 2\sum_{l=1}^{L} a_{L,l}\sum_{k=0}^{l-1}\frac{\rho|_{m-k}+\rho|_{m-k+l}}{2}\frac{u_i|_{m-k}+u_i|_{m-k+l}}{2}\frac{u_j|_{m-k}+u_j|_{m-k+l}}{2}, \tag{44}$$

respectively. Their robustness and KEP property have been demonstrated in numerical tests [2,22,57]. Another group tested by Kuya et al. [22] is:

$$\hat{C}_j|_{m+\frac{1}{2}} = 2\sum_{l=1}^{L} a_{L,l}\sum_{k=0}^{l-1}\frac{(\rho u_j)|_{m-k}+(\rho u_j)|_{m-k+l}}{2}, \tag{45}$$

$$\hat{M}_{ij}|_{m+\frac{1}{2}} = 2\sum_{l=1}^{L} a_{L,l}\sum_{k=0}^{l-1}\frac{(\rho u_j)|_{m-k}+(\rho u_j)|_{m-k+l}}{2}\frac{u_i|_{m-k}+u_i|_{m-k+l}}{2}, \tag{46}$$

the divergence and quadratic-split formulations, respectively, which were shown to be less stable than Eqs. (43) and (44). Additionally, the square-root density splitting proposed by Rozema et al. [23] satisfies the KEP condition, and its excellent performance has recently been demonstrated by De Michele and Coppola [35] and Kawai and Kawai [36] in ideal-gas, single-component flows. The formulation is given by

$$\hat{C}_j|_{m+\frac{1}{2}} = 2\sum_{l=1}^{L} a_{L,l}\sum_{k=0}^{l-1}\sqrt{\rho|_{m-k}\rho|_{m-k+l}}\frac{u_j|_{m-k}+u_j|_{m-k+l}}{2}, \tag{47}$$

$$\hat{M}_{ij}|_{m+\frac{1}{2}} = 2\sum_{l=1}^{L} a_{L,l} \sum_{k=0}^{l-1} \sqrt{\rho|_{m-k}\rho|_{m-k+l}} \frac{u_i|_{m-k} + u_i|_{m-k+l}}{2} \frac{u_j|_{m-k} + u_j|_{m-k+l}}{2}. \tag{48}$$

In the present study, we adopt the two groups, Eqs. (43) and (44) and Eqs. (47) and (48), for their superior performance.

3.3.2. Energy numerical fluxes

3.3.2.1. Entropy conservation. The construction of the numerical fluxes in the energy equation should aim for discrete conservation of entropy. We adopt the method due to Kuya et al. [22], which implicitly conserves entropy by solving the total energy equation with consistent numerical fluxes. This method is grounded in the 'conservation' form of the Gibbs equation from Subbareddy and Candler [20]:

$$\frac{\partial \rho s}{\partial t} + \frac{\partial \rho s u_j}{\partial x_j} = \frac{1}{T}\left(\left(sT - e - \frac{p}{\rho}\right)\left(\frac{\partial \rho}{\partial t} + \frac{\partial \rho u_j}{\partial x_j}\right) + \left(\frac{\partial \rho e}{\partial t} + \frac{\partial \rho e u_j}{\partial x_j} + p\frac{\partial u_j}{\partial x_j}\right)\right), \tag{49}$$

where $s = C_v \ln(p/\rho^\gamma)$ is the mixture specific entropy. This equation (Eq. (49)) suggests that entropy is implicitly conserved upon satisfying the continuity and internal energy equations. The continuity equation is satisfied discretely by solving Eq. (14), while the satisfaction of the internal energy equation follows from satisfying the total energy and the kinetic energy equations, as per:

$$\frac{\partial \rho e}{\partial t} + \frac{\partial \rho e u_j}{\partial x_j} + p\frac{\partial u_j}{\partial x_j} = \left(\frac{\partial \rho E}{\partial t} + \frac{\partial \rho E u_j}{\partial x_j} + \frac{\partial p u_j}{\partial x_j}\right) - \left(\frac{\partial \rho k}{\partial t} + \frac{\partial \rho k u_j}{\partial x_j} + u_j\frac{\partial p}{\partial x_j}\right). \tag{50}$$

Consistent numerical fluxes, i.e., fluxes satisfying the *Analytical Relations*[3] proposed by Kuya et al. [22], are required for all convective terms in Eq. (50) to maintain correct local exchanges between internal energy and kinetic energy discretely and thus conserve entropy. Interested readers are referred to Refs. [22,57] for details.

In the present study, schemes are categorised as entropy preserving, as summarised later in Table 1, if they conserve entropy in the sense of Kuya et al. [22], that is, if they use consistent numerical fluxes that satisfy the *Analytical Relations* as defined by Kuya et al. [22]. However, this approach does not strictly guarantee exact entropy conservation, as it does not directly solve the entropy equation. Consequently, some entropy conservation errors are expected, and their magnitudes may vary significantly between schemes, as suggested by the error analysis in Tamaki et al. [32]. The actual entropy-conservation properties of the schemes considered will be assessed through the numerical tests in Section 4.1.

As per Refs. [22,57], for the total energy equation (Eq. (18)), the consistent kinetic energy numerical flux $\hat{K}_j$, based on $\hat{C}_j$ and $\hat{M}_{ij}$ from Eqs. (43) and (44), respectively, is formulated as:

$$\hat{K}_j|_{m+\frac{1}{2}} = 2\sum_{l=1}^{L} a_{L,l} \sum_{k=0}^{l-1} \frac{\rho|_{m-k} + \rho|_{m-k+l}}{2} \frac{u_i|_{m-k}u_i|_{m-k+l}}{2} \frac{u_j|_{m-k} + u_j|_{m-k+l}}{2}. \tag{51}$$

The consistent internal energy numerical flux $\hat{I}_j$ takes the cubic-split form:

$$\hat{I}_j|_{m+\frac{1}{2}} = 2\sum_{l=1}^{L} a_{L,l} \sum_{k=0}^{l-1} \frac{\rho|_{m-k} + \rho|_{m-k+l}}{2} \frac{e|_{m-k} + e|_{m-k+l}}{2} \frac{u_j|_{m-k} + u_j|_{m-k+l}}{2}. \tag{52}$$

However, relaxing the consistency condition in *Analytical Relation* 2 from Refs. [22,57] to

$$\frac{\partial \rho k u_j}{\partial x_j} + \frac{\partial \rho e u_j}{\partial x_j} = \frac{\partial (\rho k + \rho e) u_j}{\partial x_j}, \tag{53}$$

allows for different splitting methods in $\hat{I}_j$ (ρ and e) and $\hat{K}_j$ (ρ and k), while still imposing the restriction that u_j be consistently split in both. This flexibility permits the inclusion of the quadratic-split form:

$$\hat{I}_j|_{m+\frac{1}{2}} = 2\sum_{l=1}^{L} a_{L,l} \sum_{k=0}^{l-1} \frac{(\rho e)|_{m-k} + (\rho e)|_{m-k+l}}{2} \frac{u_j|_{m-k} + u_j|_{m-k+l}}{2}. \tag{54}$$

This is the pressure-equilibrium-preserving flux derived by Shima et al. [31] and Jain and Moin [30], and will be discussed in the next section. The consistent numerical flux for the pressure-diffusion term $\hat{D}_j$ is in the product-rule form:

$$\hat{D}_j|_{m+\frac{1}{2}} = 2\sum_{l=1}^{L} a_{L,l} \sum_{k=0}^{l-1} \frac{p|_{m-k+l}u_j|_{m-k} + p|_{m-k}u_j|_{m-k+l}}{2}, \tag{55}$$

which is derived from the numerical flux for $\partial p/\partial x_j$ in Eq. (15):

$$\hat{G}|_{m+\frac{1}{2}} = 2\sum_{l=1}^{L} a_{L,l} \sum_{k=0}^{l-1} \frac{p|_{m-k} + p|_{m-k+l}}{2}, \tag{56}$$

[3] The *Analytical Relations* are: 1. the kinetic energy equation is derived from the continuity and momentum equations; 2. the kinetic and internal energies are convected by the same velocity; 3. the pressure-diffusion term is the sum of $u_j\partial p/\partial x_j$ in the kinetic energy equation and $p\partial u_j/\partial x_j$ in the internal energy equation [22].

and the numerical flux for $\partial u_j/\partial x_j$ in Eq. (20):

$$\hat{U}_j|_{m+\frac{1}{2}} = 2\sum_{l=1}^{L} a_{L,l} \sum_{k=0}^{l-1} \frac{u_j|_{m-k} + u_j|_{m-k+l}}{2}. \tag{57}$$

Therefore, Eqs. (51), (52), and (55) are the consistent numerical fluxes from Kuya et al. [22,57] and referred to as the KEEP scheme. The group with Eqs. (51), (54), and (55) is the KEEP$_{\text{PE}}$ scheme [31]. This methodology implies that replacing the total energy equation with the internal energy equation for entropy conservation, as in Coppola et al. [21], appears unnecessary if the consistency conditions are discretely guaranteed. When consistent numerical fluxes are used, solving both equations is equivalent in the semi-discrete limit [35].

Furthermore, the split forms of Rozema et al. [23] are also consistent numerical fluxes and demonstrate entropy conservation in a manner similar to the KEEP scheme of Kuya et al. [22]. From the total mass ($\hat{C}_j$) and momentum ($\hat{M}_{ij}$) fluxes, Eqs. (47) and (48), respectively, the consistent kinetic energy and internal energy numerical fluxes then follow as

$$\hat{K}_j|_{m+\frac{1}{2}} = 2\sum_{l=1}^{L} a_{L,l} \sum_{k=0}^{l-1} \sqrt{\rho|_{m-k}\rho|_{m-k+l}}\frac{u_i|_{m-k}u_i|_{m-k+l}}{2}\frac{u_j|_{m-k} + u_j|_{m-k+l}}{2}, \tag{58}$$

$$\hat{I}_j|_{m+\frac{1}{2}} = 2\sum_{l=1}^{L} a_{L,l} \sum_{k=0}^{l-1} \sqrt{\rho|_{m-k}\rho|_{m-k+l}}\sqrt{e|_{m-k}e|_{m-k+l}}\frac{u_j|_{m-k} + u_j|_{m-k+l}}{2}. \tag{59}$$

The consistent numerical flux for the pressure-diffusion term is subsequently given by Eq. (55). Since the scheme of Rozema et al. is KEP [23], shows excellent entropy-conservation property [35,36], and also preserves pressure equilibrium [34,36], the set with Eqs. (58), (59), and (55) is hereafter referred to as the KEEP$_{\text{PE}}$-R scheme.

Comparatively, Pirozzoli [2] adopted the total enthalpy splitting (Eq. (19)) with the cubic-split form for the total enthalpy numerical flux $\hat{H}_j$:

$$\hat{H}_j|_{m+\frac{1}{2}} = 2\sum_{l=1}^{L} a_{L,l} \sum_{k=0}^{l-1} \frac{\rho|_{m-k} + \rho|_{m-k+l}}{2}\frac{H|_{m-k} + H|_{m-k+l}}{2}\frac{u_j|_{m-k} + u_j|_{m-k+l}}{2}. \tag{60}$$

This scheme, hereafter referred to as Kennedy–Gruber–Pirozzoli (KGP) (cf. Coppola et al. [21]), does not conserve entropy and will be discussed in the numerical tests to highlight the role of entropy conservation.

3.3.2.2. Pressure-equilibrium preservation. For flows with spatially uniform pressure and velocity at the initial time, this uniformity is required to be maintained discretely with time. Shima et al. [31] proposed the pressure-equilibrium-preserving internal energy numerical flux (Eq. (54)) for a single-component flow with an initially non-uniform density field, and Jain and Moin [30] derived the same formulation for a two-phase flow. The splitting of Rozema et al. [23] based on square-root variables is also an excellent PEP scheme as demonstrated by De Michele and Coppola [34] and Kawai and Kawai [36]. However, these numerical fluxes have not been evaluated in multi-component flows with potentially varying specific heats. In the following, we discuss its applicability to multi-component flows in terms of maintaining the pressure equilibrium.

As discussed previously, the semi-discrete internal energy equation (Eq. (20)) can be derived assuming consistent numerical fluxes. For the KEEP$_{\text{PE}}$ scheme of Shima et al. [31], substituting $\hat{I}_j$ and $\hat{U}_j$ with Eqs. (54) and (57), respectively, and invoking the equation of state (Eq. (11)), the internal energy equation leads to the pressure evolution:

$$\begin{aligned}\Delta x_j \left.\frac{\partial \frac{p}{\gamma-1}}{\partial t}\right|_m = -2\sum_{l=1}^{L} a_{L,l} \sum_{k=0}^{l-1}\Bigg(&\Big(\widetilde{u_j, p, \frac{1}{\gamma-1}}\Big)^{\text{Quadratic-split}}_{m-k,l} - \Big(\widetilde{u_j, p, \frac{1}{\gamma-1}}\Big)^{\text{Quadratic-split}}_{m-1-k,l} \\ &- p|_m \frac{u_j|_{m-k} + u_j|_{m-k+l} - u_j|_{m-1-k} - u_j|_{m-1-k+l}}{2}\Bigg).\end{aligned} \tag{61}$$

Introducing an index t_n to denote that the temporal derivative and other quantities are evaluated at time step t_n, and assuming $u_j|_m^{t_n} = u_{j0}$ and $p|_m^{t_n} = p_0$, $\forall m$, we can formulate Eq. (61) as:

$$\left.\Delta x_j \frac{\partial \frac{p}{\gamma-1}}{\partial t}\right|_m^{t_n} = -2p_0u_{j0}\sum_{l=1}^{L} a_{L,l} \sum_{k=0}^{l-1}\left(\left(\widetilde{\frac{1}{\gamma-1}, 1, 1}\right)_{m-k,l} - \left(\widetilde{\frac{1}{\gamma-1}, 1, 1}\right)_{m-1-k,l}\right)\Bigg|^{t_n}, \tag{62}$$

where the two-point operator reduces to the arithmetic mean of $1/(\gamma-1)$.

In this study, we assume calorically perfect gases, with the mixture specific heat ratio depending only on concentrations and species specific heats (Eq. (10)). For the special case with uniform γ (possibly due to $\gamma_\alpha = \text{const.}$, $\forall\alpha$ or uniform concentrations), Eq. (62) reduces to:

$$\left.\frac{\partial p}{\partial t}\right|_m^{t_n} = 0, \ \forall m, \tag{63}$$

indicating the pressure equilibrium is preserved by Eq. (54) in KEEP$_{\text{PE}}$. Similarly, for the KEEP$_{\text{PE}}$-R scheme of Rozema et al. [23], substituting $\hat{I}_j$ with Eq. (59) yields the same pressure evolution as Eq. (62). Here, the two-point operator is the geometric mean of

$1/(\gamma-1)$. Assuming uniform γ, the pressure equilibrium is also preserved by Eq. (59) in KEEP$_{\mathrm{PE}}$-R. Likewise, it is straightforward to prove that the divergence form,

$$\hat{I}_j\big|_{m+\frac{1}{2}} = 2\sum_{l=1}^{L} a_{L,l} \sum_{k=0}^{l-1} \frac{(\rho e u_j)|_{m-k} + (\rho e u_j)|_{m-k+l}}{2}, \tag{64}$$

preserves the pressure equilibrium with uniform γ, whereas the cubic-split form Eq. (52) in the KEEP scheme is incapable of this. In general multi-component systems with varying γ, Eq. (63) holds if and only if an additional advection equation,

$$\frac{\partial}{\partial t}\left(\frac{1}{\gamma-1}\right) + u_j \frac{\partial}{\partial x_j}\left(\frac{1}{\gamma-1}\right) = 0, \tag{65}$$

is satisfied using the same discretisation as that used in Eq. (62). To prove this, we begin with the semi-discrete representation of Eq. (65):

$$\Delta x_j \frac{\partial \frac{1}{\gamma-1}}{\partial t}\bigg|_m^{t_n} = -2u_{j0} \sum_{l=1}^{L} a_{L,l} \sum_{k=0}^{l-1} \left(\left(\widetilde{\frac{1}{\gamma-1}}, 1, 1\right)_{m-k,l} - \left(\widetilde{\frac{1}{\gamma-1}}, 1, 1\right)_{m-1-k,l} \right)\bigg|_m^{t_n}. \tag{66}$$

Next, we apply the product rule to the temporal derivative in Eq. (62), resulting in:

$$\frac{\partial}{\partial t}\left(\frac{p}{\gamma-1}\right)\bigg|_m^{t_n} = p_0 \frac{\partial}{\partial t}\left(\frac{1}{\gamma-1}\right)\bigg|_m^{t_n} + \left(\frac{1}{\gamma-1}\right)\bigg|_m^{t_n} \frac{\partial p}{\partial t}\bigg|_m^{t_n}. \tag{67}$$

Multiplying Eq. (66) by p_0 and subtracting it from Eq. (62) leads to Eq. (63). To prove the reverse direction, i.e., deriving Eq. (66) from Eq. (63), we multiply Eq. (67) by Δx_j and substitute the terms $\Delta x_j\, \partial(p/(\gamma-1))/\partial t|_m^{t_n}$ and $\partial p/\partial t|_m^{t_n}$ using Eq. (62) and Eq. (63), respectively. The resulting relation is Eq. (66), provided $p_0 \neq 0$. Furthermore, invoking Eq. (10) shows that the $1/(\gamma-1)$ advection equation (Eq. (65)) can be satisfied by consistently satisfying the X_α advection equation for all species. Otherwise, the pressure equilibrium depends on the velocity equilibrium (as indicated by Eq. (61)), and vice versa. The KEP schemes derived from Theorem 1 ensure the preservation of velocity equilibrium (see Appendix B for the proof).

Therefore, the split numerical fluxes proposed by Shima et al. [31] and Jain and Moin [30] (Eq. (54)) and Rozema et al. [23] (Eq. (59)) can preserve pressure equilibrium only for flows with uniform specific heat ratios. For flows with varying specific heat ratios, preserving pressure equilibrium requires satisfying an additional advection equation of the material property $1/(\gamma-1)$. It is worth noting that the above analysis does not account for temperature-dependent specific heats and, therefore, does not naturally extend to a thermally perfect setting.

Directly solving the advection equation of $1/(\gamma-1)$ is a common approach to reducing spurious pressure oscillations at material interfaces [40,41,59]. Nevertheless, Johnsen and Ham [40] pointed out an inconsistency between the solutions determined by species mass fractions and those determined by $1/(\gamma-1)$. This issue is particularly relevant to finite-difference methods where pointwise values are directly concerned, although finite-volume methods might allow for variations in cell averages. Solving the advection equations of X_α implies not solving the conservative equations of ρY_α, which potentially compromises species mass conservation. The 'double-flux' model [38,39] is another approach to addressing such pressure oscillations. However, Subbareddy et al. [48] observed high energy conservation errors with this model, despite the fact that it did preserve the expected thermodynamic equilibrium. A recent study by Fujiwara et al. [42] implicitly satisfied the advection equation of $1/(\gamma-1)$ using a compatibility condition between the numerical fluxes of internal energy and species mass. As a result, their method preserves pressure equilibrium across discontinuity-free interfaces for calorically perfect gases and conserves all primary variables, without solving additional equations.

The present study will not further address numerical treatments for preserving pressure equilibrium in flows with varying specific heat ratios. Instead, our focus is on evaluating exemplary split-form PEP schemes in the context of multi-component flows. In Section 4.1, we validate the above analysis through numerical tests and evaluate the performance of the KEEP$_{\mathrm{PE}}$ and KEEP$_{\mathrm{PE}}$-R schemes, comparing them with other schemes that have different properties (e.g., KGP and KEEP). The multi-component PEP scheme of Fujiwara et al. [42], referred to here as PE-F, is also included for comparative evaluation. While its PEP property and stability have been demonstrated for calorically perfect, multi-component problems [42,46], other properties, such as entropy conservation, have not been examined.

The numerical fluxes of the PE-F scheme are:

$$\hat{C}_j\big|_{m+\frac{1}{2}} = 2\sum_{l=1}^{L} a_{L,l} \sum_{k=0}^{l-1} \frac{\phi^-\rho|_{m-k} + \phi^+\rho|_{m-k+l}}{2} \frac{u_j|_{m-k} + u_j|_{m-k+l}}{2}, \tag{68}$$

$$\hat{M}_{ij}\big|_{m+\frac{1}{2}} = 2\sum_{l=1}^{L} a_{L,l} \sum_{k=0}^{l-1} \frac{\phi^-\rho|_{m-k} + \phi^+\rho|_{m-k+l}}{2} \frac{u_i|_{m-k} + u_i|_{m-k+l}}{2} \frac{u_j|_{m-k} + u_j|_{m-k+l}}{2}, \tag{69}$$

$$\hat{K}_j\big|_{m+\frac{1}{2}} = 2\sum_{l=1}^{L} a_{L,l} \sum_{k=0}^{l-1} \frac{\phi^-\rho|_{m-k} + \phi^+\rho|_{m-k+l}}{2} \frac{u_i|_{m-k}u_i|_{m-k+l}}{2} \frac{u_j|_{m-k} + u_j|_{m-k+l}}{2}, \tag{70}$$

where $\phi^- = \frac{W|_{m-k}}{\rho|_{m-k}} \frac{\rho|_{m-k+l}}{W|_{m-k+l}}$ and $\phi^+ = \frac{W|_{m-k+l}}{\rho|_{m-k+l}} \frac{\rho|_{m-k}}{W|_{m-k}}$. The formulations of $\hat{G}$, $\hat{I}_j$, and $\hat{D}_j$ are the same as those of the KEEP_{PE} scheme, i.e., Eqs. (56), (54), and (55), respectively. The species mass numerical flux $\hat{Y}_{\alpha,j}$, $\alpha = 1, \cdots, N_s - 1$, of PE-F is expressed as:

$$\hat{Y}_{\alpha,j}|_{m+\frac{1}{2}} = 2 \sum_{l=1}^{L} a_{L,l} \sum_{k=0}^{l-1} \frac{(\phi^- \rho Y_\alpha)|_{m-k} + (\phi^+ \rho Y_\alpha)|_{m-k+l}}{2} \frac{u_j|_{m-k} + u_j|_{m-k+l}}{2}, \tag{71}$$

which was constructed from the compatibility condition of pressure equilibrium [42]. Note that the species fluxes for the KEEP_{PE} and KEEP_{PE}-R schemes take different forms and will be constructed in the following section.

It is evident that $\hat{C}_j$ and $\hat{M}_{ij}$ of the PE-F scheme satisfy the KEP condition. However, since the density averages in the PE-F scheme are weighted by the mixture molar mass (W), variations in W can influence the solutions for density and other flow variables. This effect can be exemplified by a simplified one-dimensional case with uniform density and velocity at time step t_n, i.e., $u|_m^{t_n} = u_0$ and $\rho|_m^{t_n} = \rho_0$, $\forall m$. In this setting, the continuity equation (Eq. (1)) suggests that the density remains constant in time: $\partial\rho/\partial t|_m^{t_n} = -\partial\rho_0 u_0/\partial x|_m^{t_n} = 0$, $\forall m$. However, applying the semi-discrete continuity equation (Eq. (14)) with the PE-F total mass flux (Eq. (68)) yields

$$\Delta x \frac{\partial \rho}{\partial t}\bigg|_m^{t_n} = -\rho_0 u_0 \sum_{l=1}^{L} a_{L,l} \sum_{k=0}^{l-1} \left(\frac{W|_{m-k}}{W|_{m-k+l}} + \frac{W|_{m-k+l}}{W|_{m-k}} - \frac{W|_{m-k-1}}{W|_{m-k+l-1}} - \frac{W|_{m-k+l-1}}{W|_{m-k-1}} \right)\bigg|^{t_n}, \tag{72}$$

which shows that $\partial\rho/\partial t|_m^{t_n} = 0$, $\forall m$ is not ensured for non-uniform W, as spatial variation in W leads to imbalanced contributions in the flux evaluation. This example therefore suggests that the total mass flux $\hat{C}_j$ in PE-F may introduce density errors, with their magnitudes depending directly on the point-to-point variation of W across the grid. Additionally, while PE-F satisfies the *Analytical Relations* in a manner similar to KEEP_{PE}, the use of inconsistent density averages in $\hat{K}_j$ and $\hat{I}_j$ under varying W conditions may also introduce additional entropy conservation errors. These characteristics will be evaluated in numerical tests in Section 4.1.

3.3.3. Species mass numerical fluxes

This section constructs the numerical flux for species mass ($\hat{Y}_{\alpha,j}$) based on the physical properties of preserving the uniform distributions of species mass fraction and temperature under relevant conditions.

3.3.3.1. Uniform species mass fraction preservation. For flows with spatially uniform species mass fractions for any species α at the initial time, such uniform distributions should be preserved in time. This is indicated by the evolution equation of species mass fractions,

$$\frac{\partial Y_\alpha}{\partial t} = \frac{1}{\rho}\left(\frac{\partial \rho Y_\alpha}{\partial t} - Y_\alpha \frac{\partial \rho}{\partial t} \right) = \frac{1}{\rho}\left(Y_\alpha \frac{\partial \rho u_j}{\partial x_j} - \frac{\partial \rho Y_\alpha u_j}{\partial x_j} \right), \ \alpha = 1, \cdots, N_s - 1, \tag{73}$$

which are derived from the species equation (Eq. (4)) and the continuity equation (Eq. (1)). With the condition $Y_\alpha|_m^{t_n} = Y_{\alpha 0}$, $\forall m$, the temporal derivative at time step t_n reduces to zero:

$$\frac{\partial Y_\alpha}{\partial t}\bigg|_m^{t_n} = \frac{1}{\rho|_m^{t_n}} \left(Y_{\alpha 0} \frac{\partial \rho u_j}{\partial x_j}\bigg|_m^{t_n} - \frac{\partial \rho Y_{\alpha 0} u_j}{\partial x_j}\bigg|_m^{t_n} \right) = 0, \ \forall m, \forall \alpha \in [1 \,..\, N_s - 1]. \tag{74}$$

It should be noted that Eq. (73) is analytically equivalent to the advection equation of mass fraction ($\partial Y_\alpha/\partial t = -u_j \partial Y_\alpha/\partial x_j$), which suggests the same constraint as Eq. (74). Summing Eq. (73) over $N_s - 1$ species and subtracting it from $\partial \sum_{\alpha=1}^{N_s} Y_\alpha/\partial t = 0$ indicates that Eq. (74) applies to species N_s.

However, under non-uniform density and velocity conditions, this uniform distribution of mass fraction may not be preserved by some split formulations, due to inconsistency between formulations for total mass and species mass. Hence, we propose a consistency condition in Theorem 2, the satisfaction of which yields numerical flux formulations that preserve uniform mass fractions. Its proof is presented subsequently.

Theorem 2. *In an inviscid, compressible, N_s-species flow ($\sum_{\alpha=1}^{N_s} Y_\alpha = 1$), if any species $\alpha \in [1 \,..\, N_s]$ has a spatially uniform mass fraction at time step t_n, i.e., $Y_\alpha|_m^{t_n} = Y_{\alpha 0}$, $\forall m$, the uniformity of mass fraction Y_α is preserved in the semi-discrete sense, if the numerical flux for the species mass,*

$$\hat{Y}_{\alpha,j}|_{m+\frac{1}{2}} = 2 \sum_{l=1}^{L} a_{L,l} \sum_{k=0}^{l-1} (\widetilde{\rho, u_j, Y_\alpha})_{m-k,l}, \ \forall \alpha \in [1 \,..\, N_s - 1], \tag{75}$$

is consistent with the numerical flux for the total mass,

$$\hat{C}_j|_{m+\frac{1}{2}} = 2 \sum_{l=1}^{L} a_{L,l} \sum_{k=0}^{l-1} (\widetilde{\rho, u_j, 1})_{m-k,l}, \tag{76}$$

that is, the following condition is satisfied:

$$(\widetilde{\rho, u_j, 1})_{m-k,l} - (\widetilde{\rho, u_j, Y_\alpha})_{m-k,l} = (\rho, \widetilde{u_j, 1 - Y_\alpha})_{m-k,l}, \ \forall \alpha \in [1 \,..\, N_s - 1], \tag{77}$$

where the two-point discrete averaging operators, $\widetilde{(\cdot,\cdot,\cdot)}$, are defined in Eqs. (34)–(38).

Proof. We start from the semi-discrete equation of Eq. (73), for any $\alpha = 1, \cdots, N_s - 1$,

$$\left.\frac{\partial Y_\alpha}{\partial t}\right|_m = \frac{1}{\rho|_m}\left(Y_\alpha|_m \frac{\hat{C}_j|_{m+\frac{1}{2}} - \hat{C}_j|_{m-\frac{1}{2}}}{\Delta x_j} - \frac{\hat{Y}_{\alpha,j}|_{m+\frac{1}{2}} - \hat{Y}_{\alpha,j}|_{m-\frac{1}{2}}}{\Delta x_j}\right). \tag{78}$$

Substituting for $\hat{C}_j$ and $\hat{Y}_{\alpha,j}$ using Eq. (75) and Eq. (76), respectively, and applying the condition $Y_\alpha|_m^{t_n} = Y_{\alpha 0}$, $\forall m$, we obtain, at time step t_n, for any $\alpha = 1, \cdots, N_s - 1$,

$$\Delta x_j \left.\frac{\partial Y_\alpha}{\partial t}\right|_m^{t_n} = \frac{1}{\rho|_m^{t_n}} 2 \sum_{l=1}^{L} a_{L,l} \sum_{k=0}^{l-1} \left(Y_{\alpha 0}(\widetilde{\rho, u_j, 1})_{m-k,l} - (\widetilde{\rho, u_j, Y_{\alpha 0}})_{m-k,l} - Y_{\alpha 0}(\widetilde{\rho, u_j, 1})_{m-1-k,l} + (\widetilde{\rho, u_j, Y_{\alpha 0}})_{m-1-k,l} \right)\Bigg|^{t_n}. \tag{79}$$

Invoking the consistency condition Eq. (77) and the relation $Y_{\alpha 0}(\widetilde{\rho, u_j, 1})_{m-k,l} = (\widetilde{\rho, u_j, Y_{\alpha 0} \cdot 1})_{m-k,l}$, we obtain, for any $\alpha = 1, \cdots, N_s - 1$,

$$\Delta x_j \left.\frac{\partial Y_\alpha}{\partial t}\right|_m^{t_n} = \frac{1}{\rho|_m^{t_n}} 2 \sum_{l=1}^{L} a_{L,l} \sum_{k=0}^{l-1} \left((\widetilde{\rho, u_j, Y_{\alpha 0} - Y_{\alpha 0}})_{m-k,l} - (\widetilde{\rho, u_j, Y_{\alpha 0} - Y_{\alpha 0}})_{m-1-k,l} \right)\Bigg|^{t_n} = 0, \ \forall m. \tag{80}$$

Then we prove this for species N_s. Summing Eq. (78) over all $N_s - 1$ species and implementing Eqs. (75) and (76) for all $N_s - 1$ species, we obtain, at time step t_n,

$$\begin{aligned}\Delta x_j \left.\frac{\partial \sum_{\alpha=1}^{N_s-1} Y_\alpha}{\partial t}\right|_m^{t_n} = \frac{1}{\rho|_m^{t_n}} 2 \sum_{l=1}^{L} a_{L,l} \sum_{k=0}^{l-1} \Bigg(& \sum_{\alpha=1}^{N_s-1} Y_\alpha|_m^{t_n} (\widetilde{\rho, u_j, 1})_{m-k,l} - \sum_{\alpha=1}^{N_s-1} (\widetilde{\rho, u_j, Y_\alpha})_{m-k,l} - \sum_{\alpha=1}^{N_s-1} Y_\alpha|_{m-1}^{t_n} (\widetilde{\rho, u_j, 1})_{m-1-k,l} \\ & + \sum_{\alpha=1}^{N_s-1} (\widetilde{\rho, u_j, Y_\alpha})_{m-1-k,l} \Bigg)\Bigg|^{t_n}.\end{aligned} \tag{81}$$

Applying the consistency condition Eq. (77) for all $N_s - 1$ species, we obtain the relation $(\widetilde{\rho, u_j, 1})_{m-k,l} - \sum_{\alpha=1}^{N_s-1} (\widetilde{\rho, u_j, Y_\alpha})_{m-k,l} = (\rho, u_j, \widetilde{1 - \sum_{\alpha=1}^{N_s-1} Y_\alpha})_{m-k,l}$. Using the uniformity condition for $\alpha = N_s$ ($Y_{N_s}|_m^{t_n} = Y_{N_s 0}$, $\forall m$), we have $\sum_{\alpha=1}^{N_s-1} Y_\alpha|_m^{t_n} = 1 - Y_{N_s 0}$, $\forall m$. Hence, Eq. (81) equals 0. Given $Y_{N_s} = 1 - \sum_{\alpha=1}^{N_s-1} Y_\alpha$, we arrive at the equilibrium for species N_s:

$$\Delta x_j \left.\frac{\partial Y_{N_s}}{\partial t}\right|_m^{t_n} = \Delta x_j \left.\frac{\partial\left(1 - \sum_{\alpha=1}^{N_s-1} Y_\alpha\right)}{\partial t}\right|_m^{t_n} = 0, \ \forall m. \tag{82}$$

With Eqs. (80) and (82), we obtain, for any $\alpha = 1, \cdots, N_s$,

$$\left.\frac{\partial Y_\alpha}{\partial t}\right|_m^{t_n} = 0, \ \forall m. \tag{83}$$

□

This consistency condition (Eq. (77)) stipulates that the way that the ρ and u_j terms are formulated in $\hat{Y}_{\alpha,j}$ needs to be the same as that in $\hat{C}_j$. For the KEEP$_{\text{PE}}$ scheme, we adopt the quadratic-split form (Eq. (43)) for $\hat{C}_j$, so the forms for $\hat{Y}_{\alpha,j}$ allowed by the condition are:

$$\hat{Y}_{\alpha,j}|_{m+\frac{1}{2}} = 2 \sum_{l=1}^{L} a_{L,l} \sum_{k=0}^{l-1} \frac{\rho|_{m-k} + \rho|_{m-k+l}}{2} \frac{(u_j Y_\alpha)|_{m-k} + (u_j Y_\alpha)|_{m-k+l}}{2}, \tag{84}$$

$$\hat{Y}_{\alpha,j}|_{m+\frac{1}{2}} = 2 \sum_{l=1}^{L} a_{L,l} \sum_{k=0}^{l-1} \frac{(\rho Y_\alpha)|_{m-k} + (\rho Y_\alpha)|_{m-k+l}}{2} \frac{u_j|_{m-k} + u_j|_{m-k+l}}{2}, \tag{85}$$

$$\hat{Y}_{\alpha,j}|_{m+\frac{1}{2}} = 2 \sum_{l=1}^{L} a_{L,l} \sum_{k=0}^{l-1} \frac{\rho|_{m-k} + \rho|_{m-k+l}}{2} \frac{u_j|_{m-k} + u_j|_{m-k+l}}{2} \frac{Y_\alpha|_{m-k} + Y_\alpha|_{m-k+l}}{2}, \tag{86}$$

where the first two are quadratic-split forms and hereafter referred to as Q1 and Q2, respectively, while the last one is the cubic-split form and hereafter termed KGP. The name for the cubic-split form (KGP) follows Coppola et al. [21]. Even though the KG form (Eq. (27)) cannot be cast into a numerical flux form, it reduces to a split form that satisfies the consistency condition under uniform mass fractions. However, another quadratic-split form:

$$\hat{Y}_{\alpha,j}|_{m+\frac{1}{2}} = 2 \sum_{l=1}^{L} a_{L,l} \sum_{k=0}^{l-1} \frac{(\rho u_j)|_{m-k} + (\rho u_j)|_{m-k+l}}{2} \frac{Y_\alpha|_{m-k} + Y_\alpha|_{m-k+l}}{2}, \tag{87}$$

and the divergence form:

$$\hat{Y}_{\alpha,j}|_{m+\frac{1}{2}} = 2 \sum_{l=1}^{L} a_{L,l} \sum_{k=0}^{l-1} \frac{(\rho u_j Y_\alpha)|_{m-k} + (\rho u_j Y_\alpha)|_{m-k+l}}{2}, \tag{88}$$

do not satisfy the consistency condition. They will be included in the numerical test to highlight the role of satisfying this condition for preserving uniform mass fraction. The form Eq. (87) is referred to as Q3, while the divergence form Eq. (88) is termed DIV, which is equivalent to the standard central-difference scheme.

Nevertheless, the consistency condition also suggests that if the total mass numerical flux ($\hat{C}_j$) adopts the divergence form (Eq. (45)), the quadratic-split form Q3 and the divergence form DIV can preserve uniform mass fraction, where the latter is commonly employed in compressible solvers. Conversely, the Q1, Q2 and KGP forms do not satisfy the condition with the divergence-form total mass numerical flux.

For the KEEP$_{\text{PE}}$-R scheme, based on the square-root form of $\hat{C}_j$ (Eq. (47)), we propose two forms for $\hat{Y}_{\alpha,j}$:

$$\hat{Y}_{\alpha,j}|_{m+\frac{1}{2}} = 2\sum_{l=1}^{L} a_{L,l} \sum_{k=0}^{l-1} \sqrt{\rho|_{m-k}\rho|_{m-k+l}}\, \frac{u_j|_{m-k} + u_j|_{m-k+l}}{2}\, \frac{Y_\alpha|_{m-k} + Y_\alpha|_{m-k+l}}{2}, \tag{89}$$

$$\hat{Y}_{\alpha,j}|_{m+\frac{1}{2}} = 2\sum_{l=1}^{L} a_{L,l} \sum_{k=0}^{l-1} \sqrt{\rho|_{m-k}\rho|_{m-k+l}}\, \frac{u_j|_{m-k} + u_j|_{m-k+l}}{2}\, \sqrt{Y_\alpha|_{m-k} Y_\alpha|_{m-k+l}}. \tag{90}$$

The first form, referred to as RA, applies the arithmetic mean to Y_α and satisfies the consistency condition. The second form, termed RG, uses the geometric mean of Y_α, resulting in the geometric mean of the partial density: $\sqrt{\rho_\alpha|_{m-k}\rho_\alpha|_{m-k+l}}$. Under the assumption $Y_\alpha|_m^{t_n} = Y_{\alpha 0}$, $\forall m$, the RG formulation satisfies the consistency condition for $\alpha = 1, \cdots, N_s - 1$. However, it does not hold for species N_s because $1 - \sum_{\alpha=1}^{N_s-1} \sqrt{Y_\alpha|_{m-k} Y_\alpha|_{m-k+l}} \neq \sqrt{Y_{N_s}|_{m-k} Y_{N_s}|_{m-k+l}}$. In Section 4.2, the performance of both RA and RG will be evaluated through numerical tests.

An alternative form, based on $\sqrt{\rho|_{m-k}\rho|_{m-k+l}}\, \frac{(u_j Y_\alpha)|_{m-k} + (u_j Y_\alpha)|_{m-k+l}}{2}$, also satisfies the consistency condition. This form yields findings similar to the Q1 form for the KEEP$_{\text{PE}}$ scheme, and therefore for simplicity, is not included in the evaluation. Other formulations that do not satisfy the consistency condition, i.e., $\sqrt{\rho u_j|_{m-k}\rho u_j|_{m-k+l}}\, \frac{Y_\alpha|_{m-k} + Y_\alpha|_{m-k+l}}{2}$ and $\sqrt{\rho u_j Y_\alpha|_{m-k}\rho u_j Y_\alpha|_{m-k+l}}$, which are similar to Q3 and DIV for the KEEP$_{\text{PE}}$ scheme, respectively, are likewise excluded.

3.3.3.2. Temperature-equilibrium preservation. The temperature prediction becomes important when extending to Navier–Stokes equations, where heat diffusion and chemical reactions are solved. In the context of Euler equations, the temperature is computed from the mixture ideal-gas law in Eq. (12), and as pointed out by Terashima et al. [41] and Subbareddy et al. [48], its solution is directly related to the mixture molar concentration ($c = \rho/W$) by

$$T = \frac{p}{R_u c}. \tag{91}$$

We can derive the transport equation of c from the species equation (Eq. (4)) and the continuity equation (Eq. (1)):

$$\frac{\partial c}{\partial t} + \frac{\partial c u_j}{\partial x_j} = 0, \tag{92}$$

which suggests that for flows with spatially uniform velocity and mixture molar concentration at any time step t_n, the uniform mixture molar concentration is preserved in time:

$$\left.\frac{\partial c}{\partial t}\right|_m^{t_n} = 0, \ \forall m. \tag{93}$$

Then, from Eq. (91), the temperature temporal evolution can be represented by

$$\frac{\partial T}{\partial t} = \frac{1}{R_u c^2}\left(c\frac{\partial p}{\partial t} - p\frac{\partial c}{\partial t}\right), \tag{94}$$

indicating that if Eq. (93) is true, the temperature should be uniform and preserved in equilibrium over time, assuming that the pressure is uniform and in equilibrium. Otherwise, any spurious oscillations in molar concentration (and pressure) will contaminate the temperature field.

Since c is the sum of species molar concentrations ($c_\alpha = \rho Y_\alpha / W_\alpha$):

$$c = \sum_{\alpha=1}^{N_s} c_\alpha = \sum_{\alpha=1}^{N_s} \frac{\rho Y_\alpha}{W_\alpha}, \tag{95}$$

the numerical treatment of ρY_α, i.e., the numerical flux for species mass, is crucial for preserving the uniform molar concentration and thereby for avoiding temperature errors. Therefore, we formulate a condition in Theorem 3 for the species mass numerical flux. The formulations satisfying this condition are able to preserve the uniform mixture molar concentration and temperature. The proof of this theorem is presented subsequently.

Theorem 3. *In an inviscid, compressible, N_s-species flow ($\sum_{\alpha=1}^{N_s} Y_\alpha = 1$), if the flow has spatially uniform velocity and mixture molar concentration at time step t_n, i.e., $u_j|_m^{t_n} = u_{j0}$ and $c|_m^{t_n} = c_0$, $\forall m$, the uniformity of the mixture molar concentration is preserved with time in the semi-discrete sense, if the numerical flux for the species mass,*

$$\hat{Y}_{\alpha,j}|_{m+\frac{1}{2}} = 2\sum_{l=1}^{L} a_{L,l} \sum_{k=0}^{l-1} \widetilde{(\rho, u_j, Y_\alpha)}_{m-k,l}, \ \forall \alpha \in [1 \,..\, N_s - 1], \tag{96}$$

satisfies the following condition for all species, $\alpha \in [1 \,..\, N_s]$:

$$(\widetilde{\rho, u_j, Y_\alpha})_{m-k,l} = (c_\alpha \widetilde{W_\alpha, u_j}, 1)_{m-k,l}, \tag{97}$$

where the two-point discrete averaging operators, $\widetilde{(\cdot,\cdot,\cdot)}$, are defined in Eqs. (34)–(37).

Proof. Starting from the semi-discrete species equation (Eq. (17)); substituting for $\hat{Y}_{\alpha,j}$ using Eq. (96) and applying the uniform velocity condition $u_j|_m^{t_n} = u_{j_0}$, $\forall m$, we obtain, at time step t_n, for all $N_s - 1$ species,

$$\Delta x_j \left.\frac{\partial \rho Y_\alpha}{\partial t}\right|_m^{t_n} = -2 \sum_{l=1}^{L} a_{L,l} \sum_{k=0}^{l-1} \left(\widetilde{(\rho, u_{j_0}, Y_\alpha)}_{m-k,l} - \widetilde{(\rho, u_{j_0}, Y_\alpha)}_{m-1-k,l} \right) \Bigg|^{t_n}. \tag{98}$$

Summing them over $N_s - 1$ species and deducting it from the semi-discrete continuity equation (Eq. (14)), we obtain the semi-discrete transport equation for species N_s. Assuming a consistent numerical flux for total mass, the equation for N_s species is in the same form as Eq. (98). For all N_s species, dividing each equation (Eq. (98)) by their respective molar mass, W_α, and applying the condition in Eq. (97), we obtain

$$\Delta x_j \left.\frac{\partial c_\alpha}{\partial t}\right|_m^{t_n} = -2 \sum_{l=1}^{L} a_{L,l} \sum_{k=0}^{l-1} \left(\widetilde{(c_\alpha, u_{j_0}, 1)}_{m-k,l} - \widetilde{(c_\alpha, u_{j_0}, 1)}_{m-1-k,l} \right) \Bigg|^{t_n}, \tag{99}$$

where $\forall \alpha \in [1 \,..\, N_s]$, $\forall m$. Summing Eq. (99) over all species, with $c = \sum_{\alpha=1}^{N_s} c_\alpha$ and $c|_m^{t_n} = c_0$, $\forall m$, we arrive at

$$\left.\frac{\partial c}{\partial t}\right|_m^{t_n} = 0, \ \forall m. \tag{100}$$

□

Assuming the pressure equilibrium is preserved and invoking Eq. (94), we eventually achieve the preservation of temperature equilibrium:

$$\left.\frac{\partial T}{\partial t}\right|_m^{t_n} = 0, \ \forall m. \tag{101}$$

The condition (Eq. (97)) stipulates that ρ and Y_α in $\hat{Y}_{\alpha,j}$ need to be reconstructed together to constitute ρ_α or c_α at every grid point. Therefore, for the KEEP$_{\text{PE}}$ scheme, only the quadratic-split form, Q2 (Eq. (85)), and the divergence form, DIV (Eq. (88)), satisfy this condition. In a finite-volume framework, Subbareddy et al. [48] made a consistent choice on reconstructing ρ and Y_α together at cell faces. Adopting a partial density structure is also a logical choice for extending entropy-conservative schemes within Tadmor's framework to multi-component systems (e.g., Peyvan et al. [44] and Ching et al. [43]).

However, for the KEEP$_{\text{PE}}$-R scheme, it remains challenging to construct a formulation that meets this condition – neither RA nor RG does. Although RG constitutes ρ_α at each grid point, this does not apply to species N_s due to the geometric mean, which may introduce temperature-equilibrium errors. Furthermore, it is important to note that the RG form can be impractical in real simulations due to potential small negative values in mass fractions (e.g., from numerical oscillations), which can cause NaN errors when taking the square root. As such, RG is not our preferred species scheme for KEEP$_{\text{PE}}$-R. Instead, RA is used for the numerical tests in Section 4.1, while the differences between the two schemes are evaluated in Section 4.2.

Consequently, the Q2 form with the KEEP$_{\text{PE}}$ scheme is the only one meeting both consistency conditions (Eqs. (77) and (97)). In the subsequent numerical tests, the ability of Q2 in preserving the physical properties will be validated, and the importance of satisfying these properties will be highlighted in comparison to schemes that do not.

It is worth noting that the PE-F scheme of Fujiwara et al. [42] reduces to KEEP$_{\text{PE}}$ with Q2 as the species mass numerical flux, under uniform mass fractions or uniform c. Therefore, it satisfies both conditions, preserving the uniform mass fractions and temperature equilibrium. In the numerical tests, PE-F is included for comparison with the proposed schemes. There might be other formulations for the PE-F scheme that satisfy these physical properties. However, constructing one would need additional consideration with respect to the compatibility condition of pressure equilibrium, which may require a redesign of other terms, such as the internal energy numerical flux. This would be a challenging task and may be considered in future work.

Although this work assumes calorically perfect gases for simplicity, it is worth noting that the requirements for species schemes may extend to thermally perfect gases.

3.4. Summary of numerical schemes

3.4.1. Continuity, momentum, and energy equations

Since the first objective of the present study is to evaluate the properties and characteristics of the pressure-equilibrium-preserving schemes in the context of compressible, multi-component flows, we compare KEEP$_{\text{PE}}$ and KEEP$_{\text{PE}}$-R with PE-F and other existing schemes in numerical tests in Section 4.1. The benchmarked schemes for the continuity, momentum, and energy equations are summarised below, and their properties are listed in Table 1. For the species equation, the Q2 numerical flux Eq. (85) is used, except for KEEP$_{\text{PE}}$-R and PE-F, where the RA form Eq. (89) and Eq. (71) are used, respectively.

Table 1
Properties satisfied (✓) or not satisfied (x) by the schemes for the continuity, momentum, and energy equations; Primary conservation refers to the conservation of total mass, momentum, and total energy; *Only total mass is conserved; Entropy preserving is defined as satisfying the *Analytical Relations* proposed by Kuya et al. [22]; The pressure-equilibrium-preserving property assumes calorically perfect, multi-component flows; ‡Under the assumption of uniform specific heats.

	DIV	KG	KGP	KEEP	KEEP_{PE}	KEEP_{PE}-R	PE-F
Primary conservation	✓	x*	✓	✓	✓	✓	✓
Kinetic energy preserving	x	x	✓	✓	✓	✓	✓
Entropy preserving	x	x	x	✓	✓	✓	✓
Pressure equilibrium preserving	✓‡	x	x	x	✓‡	✓‡	✓

- **DIV**: It directly discretises the divergence-form convective terms in Eqs. (1)–(3) by the standard explicit central-difference approximation. This constitutes the baseline reference scheme, which due to its intuitive and straightforward implementation, has been widely used in compressible flow literature [9,52,54].
- **KG**: It is the low-aliasing split form by Kennedy and Gruber [9]. It discretises the split convective terms in Eqs. (24)–(26) by the standard explicit central-difference approximation. It does not conserve primary or secondary quantities, except for total mass.
- **KGP**: It is the set of kinetic-energy-preserving numerical fluxes due to Pirozzoli [2], while it does not conserve entropy. In the continuity and momentum equations (Eqs. (14) and (15)), it employs the numerical fluxes of Eqs. (43), (44), and (56). It adopts the total energy equation of Eq. (19) and splits the total enthalpy term using Eq. (60).
- **KEEP**: It is the set of kinetic-energy-preserving, entropy-preserving numerical fluxes due to Kuya et al. [22,57]. It adopts the same formulations as KGP for the continuity and momentum equations. It adopts the total energy equation of Eq. (18) and splits the internal energy, kinetic energy, pressure-diffusion terms using Eqs. (52), (51), and (55), respectively.
- **KEEP_{PE}**: It is the set of kinetic-energy-preserving, entropy-preserving, pressure-equilibrium-preserving numerical fluxes due to Shima et al. [31]. It adopts the same formulations as KEEP except that it splits the internal energy term using Eq. (54).
- **KEEP_{PE}-R**: It is the set of kinetic-energy-preserving, entropy-preserving, pressure-equilibrium-preserving fluxes due to Rozema et al. [23]. It adopts Eqs. (47), (48), and (56) for the numerical fluxes in continuity and momentum equations. It adopts the total energy equation of Eq. (18) and splits the internal energy, kinetic energy, and pressure-diffusion terms using Eqs. (59), (58), and (55), respectively.
- **PE-F**: It is the set of pressure-equilibrium-preserving fluxes due to Fujiwara et al. [42]. It adopts formulations similar to KEEP_{PE}, except using Eqs. (68) and (69) for the total mass and momentum numerical fluxes, respectively, and Eq. (70) for the kinetic energy flux.

3.4.2. Species equation

Our second objective is to demonstrate the ability of the species mass numerical fluxes in preserving the physical properties and to highlight the importance of using physically consistent species mass numerical fluxes in simulations of compressible multi-component flows. Hence, we compare the following species split forms in the numerical tests presented in Section 4.2. Note that DIV, KG, KGP, Q1, Q2, and Q3 adopt the KEEP_{PE} scheme to discretise the continuity, momentum, and energy equations, while RA and RG use KEEP_{PE}-R. PE-F is also included for comparison. The physical properties of the species schemes are summarised in Table 2.

- **DIV**: It directly applies the standard explicit central-difference approximation to $\partial \rho Y_a u_j / \partial x$ in Eq. (4) and is equivalent to the divergence-form numerical flux Eq. (88). This constitutes the baseline reference scheme.
- **KG**: It is the low-aliasing split form by Kennedy and Gruber [9]. It discretises the split species convective term in Eq. (27) using the standard explicit central-difference approximation. It does not conserve species mass.
- **KGP**: It applies the cubic-split numerical flux Eq. (86).
- **Q1**: It applies the quadratic-split numerical flux Eq. (84).
- **Q2**: It applies the quadratic-split numerical flux Eq. (85).
- **Q3**: It applies the quadratic-split numerical flux Eq. (87).
- **RA**: It applies the square-root numerical flux Eq. (89).
- **RG**: It applies the square-root numerical flux Eq. (90).

Table 2
Properties satisfied (✓) or not satisfied (x) by the schemes for the species equation; The properties of uniform mass fraction preserving and temperature equilibrium preserving are also subject to the scheme for the continuity equation; *Except for the last species.

	DIV	KG	KGP	Q1	Q2	Q3	RA	RG
Species mass conservation	✓	x	✓	✓	✓	✓	✓	✓
Uniform mass fraction preserving	x	✓	✓	✓	✓	x	✓	✓*
Temperature equilibrium preserving	✓	x	x	x	✓	x	x	x

4. Numerical tests

In this section, we evaluate the above-listed numerical schemes in numerical experiments. All the schemes are equipped with the eighth-order explicit central approximation[4]. To ensure clarity in the following, each test is labelled according to the combination of schemes applied to the continuity, momentum, and energy equations, as well as the species equation. For example, KEEP_{PE}-Q2 refers to the KEEP_{PE} scheme used for the first three equations and the Q2 scheme for the species equation. PE-F is labelled by its standalone name, as it is already defined as a complete multi-component scheme. The classical four-stage fourth-order Runge–Kutta scheme [60] is employed. Considering the dissipative characteristics of Runge–Kutta schemes, temporal errors can be controlled by using sufficiently small time steps [61]. For the one-dimensional (1D) cases, we use very small time steps corresponding to a Courant number of approximately 0.01, which provides temporally converged results and ensures that local temporal errors remain smaller than the eighth-order spatial discretisation errors. For the three-dimensional (3D) cases, we adopt a Courant number of approximately 0.05, where, as detailed in Appendix C, time-step convergence is obtained. Therefore, we confirm that the time steps are small enough to prevent temporal errors from affecting the results and discussion that follow, and we will not discuss the effects of time integration methods further in the present study.

4.1. Continuity, momentum, and energy equations

To evaluate the properties and characteristics of the numerical schemes for continuity, momentum, and energy equations (in Section 3.4.1) in the context of multi-component flows, we benchmark them in 1D advection problems and 3D inviscid Taylor–Green vortex flows. Additionally, we demonstrate the analysis in Section 3.3, such as the pressure-equilibrium-preserving property, holds in the numerical experiments.

4.1.1. Pressure-equilibrium preservation: 1D advection

We set up 1D advection problems of scalar waves with uniform pressure and velocity, to compare the numerical schemes regarding their performance of maintaining pressure equilibrium and numerical stability in simulations of multi-component flows. We obtain the initial conditions of density, pressure, and velocity from the single-component case by De Michele and Coppola [35]:

$$u = 1,\ p = 1,\ \rho = 1 + e^{\sin 2\pi x},$$

which is similar to the case by Shima et al. [31]. The domain spans $0 \leq x \leq 1$ with periodic boundary conditions and is discretised uniformly with 61 grid points. We then extend this case to multi-component systems by initialising species mass fractions. To evaluate the performance across different profiles of the mixture specific heat ratio, we set three two-component cases, G1, G2, and G3, with different initial species mass fraction distributions:

$$\begin{aligned}
&\text{G1}: Y_{\text{H}_2} = \left(e - e^{\sin(2\pi x)}\right)/(e - e^{-1}),\ Y_{\text{N2}} = 1 - Y_{\text{H}_2};\\
&\text{G2}: Y_{\text{H}_2} = \left(e - e^{\sin(2\pi x)}\right)/(e - e^{-1}),\ Y_{\text{H}_2\text{O}} = 1 - Y_{\text{H}_2};\\
&\text{G3}: Y_{\text{H}_2} = f(1/(\gamma - 1)),\ Y_{\text{H}_2\text{O}} = 1 - Y_{\text{H}_2}.
\end{aligned}$$

In cases G1 and G2, we apply a smooth wave to the H_2 mass fraction and adopt N_2 in G1 and H_2O in G2 as the other species. Given the material properties:

$$\begin{aligned}
(\gamma_{\text{H}_2}, \gamma_{\text{N}_2}, \gamma_{\text{H}_2\text{O}}) &= (1.4, 1.4, 1.33),\\
(W_{\text{H}_2}, W_{\text{N}_2}, W_{\text{H}_2\text{O}}) &= (0.002, 0.028, 0.018),
\end{aligned}$$

G1 presents an initially uniform γ profile, whereas G2 has a varying γ profile; correspondingly, their $1/(\gamma - 1)$ profiles are uniform for G1 and varying for G2, as shown in Fig. 1. Furthermore, given that $1/(\gamma - 1)$ is the transported quantity in Eq. (65) and its variations are closely linked to internal energy and pressure changes [40,53], we expect different pressure-equilibrium behaviours in a case with a better-resolved $1/(\gamma - 1)$ profile that has smoother transitions between grid points, compared to case G2. Hence, we set up a sinusoidal $1/(\gamma - 1)$ profile in case G3:

$$\frac{1}{\gamma - 1} = 0.5\left(\frac{1}{\gamma_{\text{H}_2\text{O}} - 1} + \frac{1}{\gamma_{\text{H}_2} - 1}\right) + 0.5\left(\frac{1}{\gamma_{\text{H}_2\text{O}} - 1} - \frac{1}{\gamma_{\text{H}_2} - 1}\right)\sin(2\pi x),$$

which features smoother transitions between grid points in $0.1 < x < 0.4$ compared to G2, while maintaining the same global extrema as G2, as illustrated in Fig. 1. The initial Y_{H_2} for G3 is then computed from $1/(\gamma - 1)$ using Eqs. (9) and (10). In addition, the three cases are suitable for assessing the performance of numerical schemes under different distributions of the mixture molar mass W, particularly for PE-F, where the density fluxes are weighted by W. As shown in Fig. 1, cases G1, G2 and G3 feature different initial profiles of W. G1 has a higher peak and thus a larger variation between points in $0.1 < x < 0.4$. The W profiles of G2 and G3 share the same extrema, while for G3, the profile is sinusoidal, with smoother transitions between points.

Fig. 2 presents the profiles of ρ, p, and Y_{H_2} at $t = 19$, when the waves are transported over 19 periods, for case G1, i.e., the case with uniform γ and $1/(\gamma - 1)$. The first two subplots in the second row are the temporal evolution of $\|\epsilon_\rho\|_1$ and $\|\epsilon_p\|_1$, which are

[4] $L = 4$: $a_{4,1} = 4/5$, $a_{4,2} = -1/5$, $a_{4,3} = 4/105$, $a_{4,4} = -1/280$.

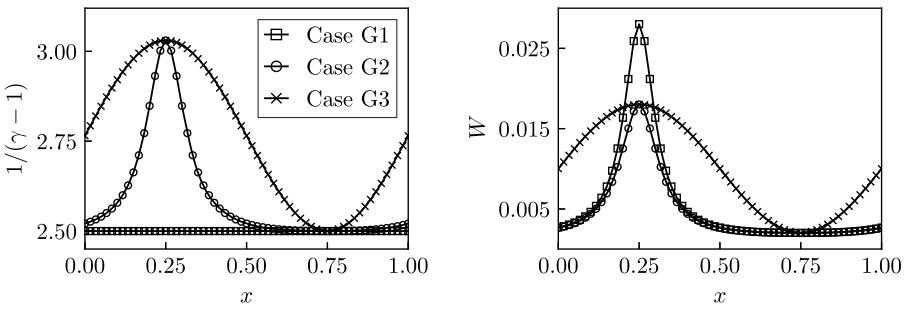

Fig. 1. The initial profiles of $1/(\gamma-1)$ and W for cases G1, G2, and G3.

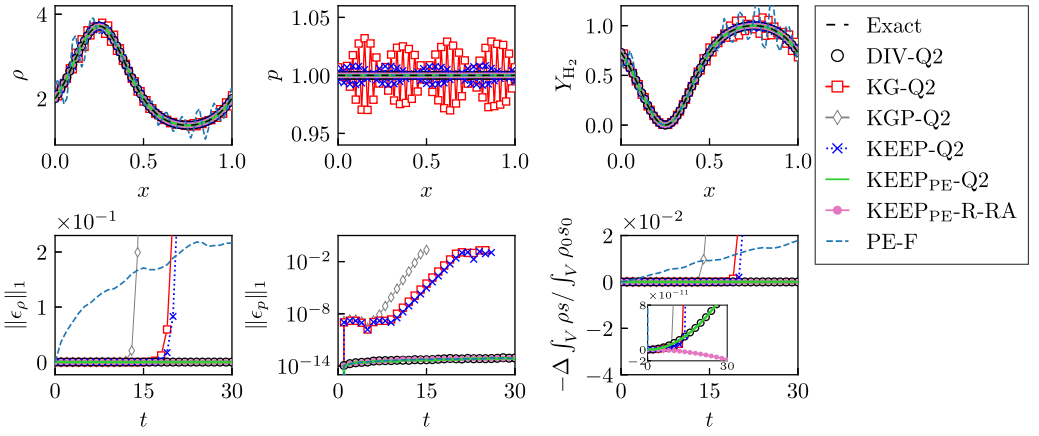

Fig. 2. The profiles for case G1: spatial distributions of density, pressure, and H_2 mass fraction at $t = 19$, and temporal evolution of density error, pressure error, and normalised entropy conservation error. The exact solution is the initial condition.

the L^1 norm of density and pressure errors, respectively. The error ϵ is defined as the deviation of the obtained solution from the exact solution: $\epsilon_{(\cdot)} = (\cdot) - (\cdot)_{\mathrm{Exact}}$. The last subplot is the temporal evolution of normalised entropy conservation error. The integration symbol $\int_V$ denotes spatial integration over the entire domain, the subscript 0 indicates the value at the initial time, and the Δ symbol indicates the change of integration from the initial time: $\Delta\int_V \rho s = \int_V \rho s - \int_V \rho_0 s_0$.

Since species mass fractions are passive scalars when γ is constant, the numerical stability from different schemes presents the same trend as the single-component flow reported by Shima et al. [31] and De Michele and Coppola [35]. The KEEP$_{\mathrm{PE}}$-Q2 and KEEP$_{\mathrm{PE}}$-R-RA schemes maintain the pressure- and velocity-equilibrium properties and achieve accurate and stable simulation in the long run[5]. Since an eighth-order spatial discretisation is used, nearly no phase errors are shown in ρ and $Y_{\mathrm{H_2}}$, unlike the second-order schemes by Shima et al. [31] and De Michele and Coppola [35] which exhibit clear phase errors. Both KEEP$_{\mathrm{PE}}$-Q2 and KEEP$_{\mathrm{PE}}$-R-RA show excellent entropy-conservation properties, with the latter producing smaller errors. Pressure oscillations emerge in the simulations using the KGP-Q2 and KEEP-Q2 schemes, and these oscillations subsequently grow exponentially, leading to the simulations blowing up at $t = 15.4$ and $t = 26.9$, respectively. Velocity oscillations (not shown in the figure) are induced through the momentum equation, and consequently, the density distribution is disturbed through the continuity equation. Both errors affect the H_2 mass fraction solution through the species mass equation.

The results for case G1 further yield new insights into the DIV-Q2, KG-Q2, and PE-F schemes. In particular, DIV-Q2 is found to preserve the pressure and velocity equilibrium. This stems from the central-difference approximation applied to the divergence-form derivatives, which subsequently leads to a numerical flux for the internal energy term in divergence form. As shown in Section 3.3.2, this divergence-form numerical flux (Eq. (64)) can preserve the pressure equilibrium (assuming γ is constant). Therefore, DIV-Q2 achieves stable and accurate simulation in the long run. However, the divergence form is usually less robust than the KGP splitting and diverges very fast in turbulent cases [2,9]. The different observations between the current and those turbulent cases may imply that preserving pressure equilibrium is critical to maintaining numerical stability in the current laminar case, but perhaps less dominant in turbulent cases.

The KG-Q2 scheme yields smaller oscillations relative to KGP-Q2 at $t = 19$. The simulation blows up at $t = 25.1$, later than KGP-Q2 but slightly earlier than KEEP-Q2. This indicates that the KG-Q2 scheme is more stable than the KGP-Q2 scheme, which is unexpected considering that KG-Q2 neither preserves kinetic energy nor inherently conserves primary variables except total mass. While Kennedy

[5] We have validated this until $t = 1000$.

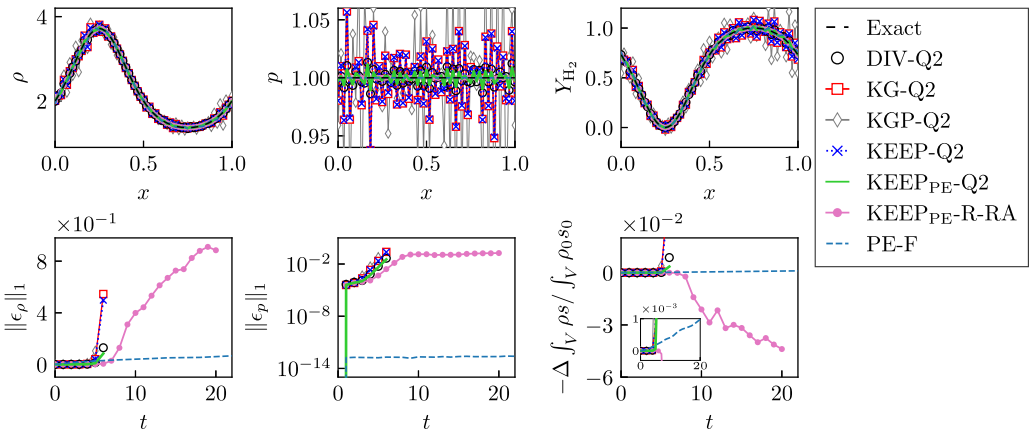

Fig. 3. The profiles for case G2: spatial distributions of density, pressure, and H_2 mass fraction at $t = 5$, and temporal evolution of density error, pressure error, and normalised entropy conservation error. The exact solution is the initial condition.

and Gruber [9] reported similar numerical stability and aliasing errors for the KG and KGP schemes tested on a 3D isotropic turbulence case, Coppola et al. [21] found for a 3D inviscid Taylor–Green vortex flow the KG scheme is less robust. However, since Coppola et al. were not using exactly the same KG scheme as in our KG-Q2 – their version, denoted as KG1, employed the product-rule form for the convective term in the continuity equation, it becomes unclear whether the improved stability observed here is specific to the current case or/and can be attributed to the difference in the continuity equation schemes. This is further discussed in the 3D inviscid Taylor–Green vortex cases in Section 4.1.2.

The PE-F scheme preserves the pressure equilibrium close to machine precision. However, it generates large oscillations in density and H_2 mass fraction. As indicated by the analysis based on Eq. (72), this behaviour results from the density averages in the flux formulations, which are weighted by the mixture molar mass at neighbouring points (e.g., in Eqs. (68) and (71)). In case G1, W is less resolved with larger point-to-point variations (see Fig. 1), which leads to imbalanced contributions in the density averages and subsequently affects the solutions for density and H_2 mass fraction. These errors grow over time and lead to entropy conservation errors in the order of 10^{-2}, which are significantly larger than those in KEEP$_{PE}$-Q2 and KEEP$_{PE}$-R-RA, eventually causing the simulation to blow up at $t = 309.1$.

Fig. 3 provides the spatial distributions at $t = 5$ and temporal evolutions for case G2, i.e., the case with varying γ and $1/(\gamma - 1)$. In this scenario, species mass fractions are no longer passive scalars as they can change the mixture specific heat ratio and hence can alter the pressure field. As analysed in Section 3.3.2, the pressure equilibrium is no longer ensured by the KEEP$_{PE}$-Q2 and KEEP$_{PE}$-R-RA schemes – spurious pressure oscillations arise at $t = 5$. These oscillations disturb the velocity equilibrium via the momentum equation, triggering oscillations in density and mass fraction and causing entropy conservation errors. The pressure oscillations intensify rapidly, resulting in a simulation failure at $t = 7.0$ for KEEP$_{PE}$-Q2. The simulation with KEEP$_{PE}$-R-RA continues to $t = 20.0$, demonstrating better stability. Similarly, the DIV-Q2 scheme fails at $t = 6.6$. Nevertheless, these three schemes still provide improved stability over KEEP-Q2, KG-Q2, and KGP-Q2, which cause the simulations to fail at $t = 6.2$, 6.1, and 5.7, respectively. These schemes follow similar relative performance to case G1 but lead to earlier simulation crashes in case G2. In contrast, the PE-F scheme maintains the pressure equilibrium to near machine precision, as it satisfies the pressure-equilibrium compatible condition regardless of the γ distribution [42]. Furthermore, due to the smaller W variations in case G2 compared to case G1, the density and mass fraction errors from the density averages in PE-F are reduced and are smaller than those caused by the pressure oscillations in KEEP$_{PE}$-Q2 and KEEP$_{PE}$-R-RA. However, these errors still induce entropy-conservation issues and lead the simulation to blow up at $t = 381.3$.

Fig. 4 provides the spatial distributions at $t = 5$ and temporal evolutions for case G3. This case also features varying γ and $1/(\gamma - 1)$, similar to G2, while G3 offers a better-resolved sinusoidal $1/(\gamma - 1)$ with smoother transitions between grid points. Compared to case G2, the KEEP$_{PE}$-Q2 and KEEP$_{PE}$-R-RA schemes exhibit noticeably improved behaviour in case G3. KEEP$_{PE}$-Q2 preserves the pressure equilibrium with an error below 10^{-5} up to $t = 70$ and sustains the simulation for about 145 periods despite subsequent error growth. KEEP$_{PE}$-R-RA maintains such approximate pressure equilibrium and numerical stability throughout the simulation ($t = 1000$). Both schemes produce only minor errors in density, mass fraction and entropy conservation. The DIV-Q2 scheme also shows enhanced stability, diverging at $t = 24.7$. These improvements are attributed to the smoother $1/(\gamma - 1)$ distribution in case G3, which reduces its jumps between grid points and subsequently lessens the pressure variations. Such $1/(\gamma - 1)$ distribution leads to a better-resolved total energy profile, which likely also mitigates the pressure oscillations. Nevertheless, the schemes that were unable to maintain pressure equilibrium in cases G1 and G2, i.e., KEEP-Q2, KG-Q2, and KGP-Q2, still lead to early simulation crashes in case G3, at respectively $t = 7.0$, 7.1, and 5.8, although the pressure oscillations are less pronounced in this case. These trends align with previous cases. The PE-F scheme retains its strong PEP property, with a smaller pressure error than in case G2. The sinusoidal W profile in case G3 also provides smoother variations between grid points, further reducing errors in density, mass fractions, and entropy conservation. Although these errors remain larger than those in KEEP$_{PE}$-Q2 and KEEP$_{PE}$-R-RA, and grow over time, the PE-F scheme achieves a stable simulation. This case highlights the potential advantage of the pressure-equilibrium-preserving numerical fluxes in

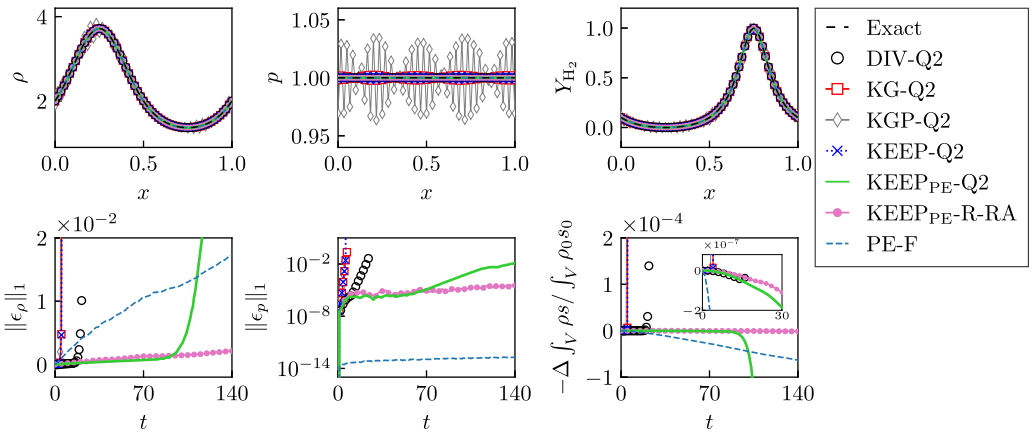

Fig. 4. The profiles for case G3: spatial distributions of density, pressure, and H_2 mass fraction at $t = 5$, and temporal evolution of density error, pressure error, and normalised entropy conservation error. The exact solution is the initial condition.

preserving pressure equilibrium and improving numerical stability in scenarios with non-uniform specific heat ratios. This finding is an important supplement to the observations from case G2.

In brief, the results from cases G1, G2, and G3 highlight that the pressure-equilibrium-preserving numerical schemes used in DIV-Q2, KEEP$_{PE}$-Q2, and KEEP$_{PE}$-R-RA cannot fully guarantee the pressure-equilibrium preservation in flows with varying specific heat ratios. Nevertheless, they still outperform schemes lacking this property. In particular, KEEP$_{PE}$-Q2 and KEEP$_{PE}$-R-RA provide better pressure-equilibrium preservation and numerical stability, especially for flows with a smooth sinusoidal $1/(\gamma - 1)$ distribution. Conversely, PE-F maintains the pressure equilibrium regardless of the γ profile and shows better stability than KEEP$_{PE}$-Q2 and KEEP$_{PE}$-R-RA in flows with varying γ. However, for flows with less resolved W profiles, PE-F introduces errors (e.g., in density and entropy conservation) that affect numerical stability.

For the cases in the following sections, we focus on physical properties beyond pressure equilibrium and consider only uniform specific heat ratios.

4.1.2. *Conservation and numerical stability: Inviscid Taylor–Green vortex*

In this section, inviscid Taylor–Green vortex (TGV) flows are examined using the numerical schemes, with the aim to compare their performance in under-resolved simulations and identify reliable schemes. Based on previous studies [22,31,35,57], our analysis includes a wider selection of schemes and considers additional metrics, including the conservation of primary invariants (see Table 1). We present all results in the eighth-order accuracy, unlike the previous second-order accuracy comparisons of KGP, KEEP, and KEEP$_{PE}$ [31]. The initial conditions for the density, velocities, pressure, and species mass fractions are given as

$$
\begin{aligned}
&\rho = 1,\\
&u = M_0 \sin(x)\cos(y)\cos(z),\\
&v = -M_0 \cos(x)\sin(y)\cos(z),\\
&w = 0,\\
&p = \frac{1}{\gamma_0} + \frac{\rho {M_0}^2}{16}\Big(\cos(2x) + \cos(2y)\Big)\Big(\cos(2z) + 2\Big),\\
&Y_{H_2} = 0.8,\\
&Y_{N_2} = 1 - Y_{H_2}.
\end{aligned}
$$

The initial mixture specific heat ratio is $\gamma_0 = \gamma_{H_2} = \gamma_{N_2} = 1.4$. The initial Mach number M_0 is set to 0.05 and 0.4 in order to model an (effectively) incompressible flow and a compressible flow, respectively. The computational domain is a triply periodic box of dimension $[0, 2\pi]^3$, discretised uniformly with 33^3 grid points. No subgrid-scale model is used. Since PE-F reduces to KEEP$_{PE}$-Q2 with uniform species mass fractions, it is not included in this evaluation. The simulations were run up to $\hat{t} = 200$, where $\hat{t} = M_0 t$ is the scaled time.

The results are shown in Figs. 5 and 6 for $M_0 = 0.05$ and $M_0 = 0.4$, respectively, in terms of temporal evolution of primary invariants (i.e., total mass, momentum, total energy, and species mass), secondary invariants (i.e., kinetic energy and entropy), and root-mean-square (rms) value of fluctuations in density, temperature, and species mass fraction. In these plots, as introduced for Fig. 2, $\int_V$ denotes spatial integration and $\Delta \int_V (\cdot) = \int_V (\cdot) - \int_V (\cdot)_0$ is the change of the integrated values compared to $\hat{t} = 0$. The overbar denotes spatial average over the domain, and the prime symbol represents the fluctuation from the average, therefore its rms: $(\cdot)'_{\text{rms}} = \sqrt{\overline{((\cdot)-\overline{(\cdot)})^2}}$.

The computations employing the DIV-Q2 scheme crash before $\hat{t} = 5$ for both M_0. Designed to reduce the aliasing errors, the KG-Q2 scheme manages to drive the computation to $\hat{t} = 200$ for $M_0 = 0.05$. KG-Q2 yields approximately the same level of fluctuations in

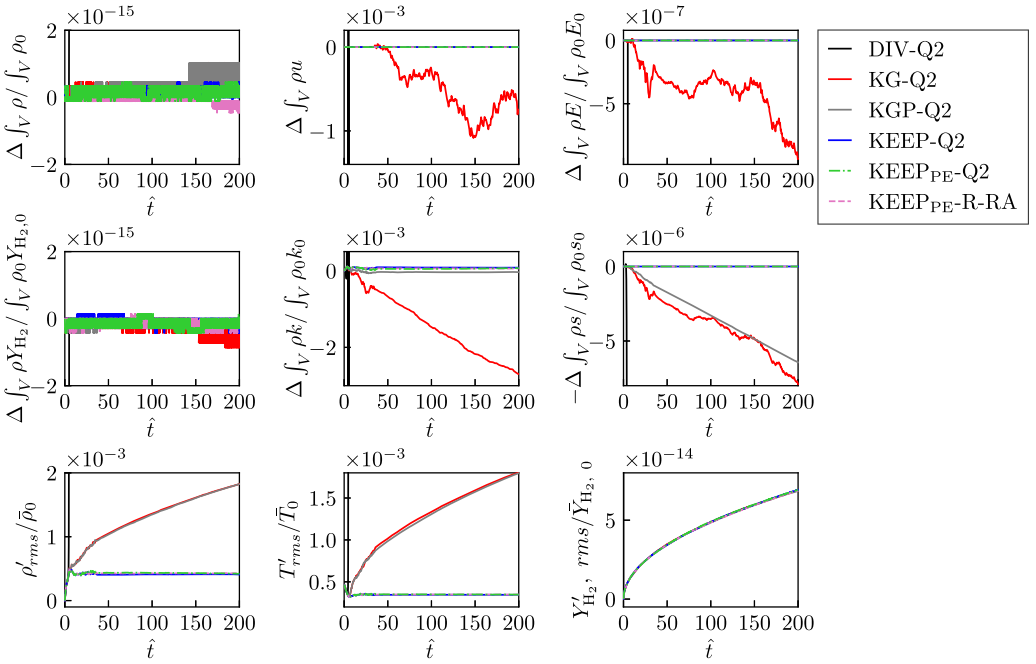

Fig. 5. Temporal evolution of primary invariants, secondary invariants, and rms value of fluctuations for the TGV flow at $M_0 = 0.05$.

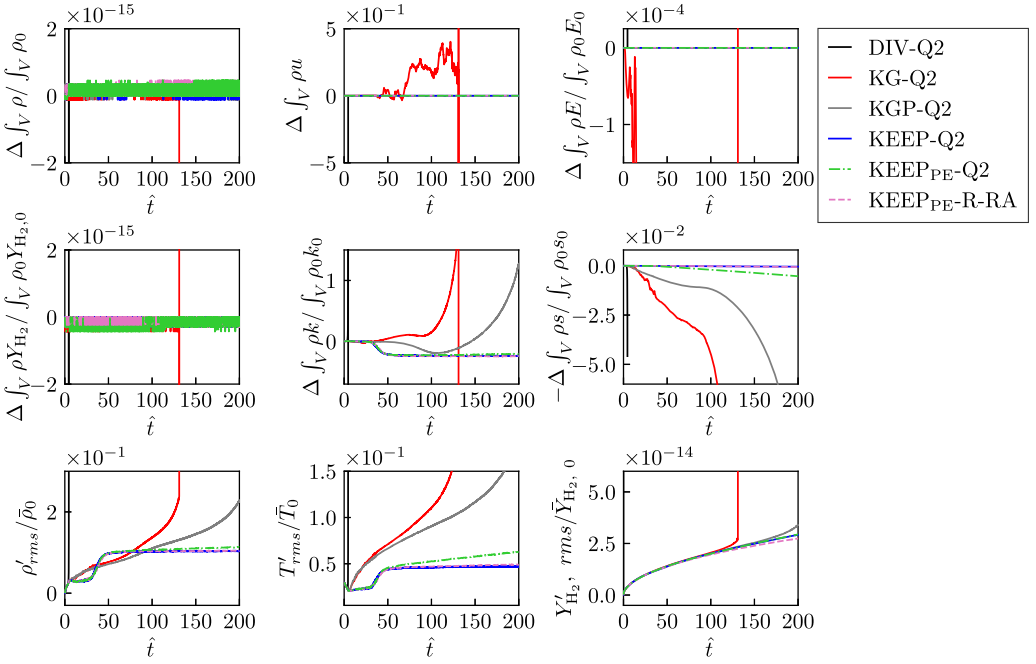

Fig. 6. Temporal evolution of primary invariants, secondary invariants, and rms value of fluctuations for the TGV flow at $M_0 = 0.4$.

density and temperature as the KGP-Q2 scheme, although it is unable to conserve the momentum, total energy, and kinetic energy, and produces larger entropy reduction than KGP-Q2. On the contrary, in the incompressible TGV test by Coppola et al. [21], their KG1 form crashes at the very beginning. As mentioned in the above section (case G1), the only difference between their KG1 form and the KG form in our KG-Q2 is the split method applied to the convective term in the continuity equation. This implies that this difference improves the stability for KG-Q2. However, for $M_0 = 0.4$, KG-Q2 is unstable – it leads to an exponential growth of kinetic energy and thermodynamic fluctuations after $\hat{t} \approx 50$ and causes the computation to crash at $\hat{t} = 131$. The KGP-Q2 form is more stable as it delays the exponential growth. This implies that the primary conservation and kinetic-energy preservation of KGP-Q2 improve

the stability in the under-resolved compressible simulation. However, this appears to be less significant in the previous well-resolved 1D cases, as KG-Q2 exhibits better stability than KGP-Q2 there. Nonetheless, it is very likely that KGP-Q2 crashes soon after $\hat{t} = 200$ given the exponential growth of kinetic energy and fluctuations.

For the KEEP-Q2 scheme, stable simulations are observed for $M_0 = 0.05$ and 0.4, where the kinetic energy and thermodynamic fluctuations reach an asymptotically constant level. This is likely attributed to the feature of KEEP-Q2 that accurately represents local energy exchanges between kinetic energy and internal energy, contributing to entropy conservation. Particularly for $M_0 = 0.4$, where higher physical compressibility causes more evident energy exchanges through the pressure work [21,22,30], the benefits of this feature is pronounced, as indicated by the improvements of KEEP-Q2 over KGP-Q2. Considering that entropy conservation is implicitly achieved by KEEP-Q2, small errors in entropy conservation should be allowed – entropy reductions of the order of 10^{-10} for $M_0 = 0.05$ and 10^{-4} for $M_0 = 0.4$ were observed. Similar levels of entropy conservation errors were also reported by Kuya et al. [22] and Shima et al. [31].

For the KEEP$_{\text{PE}}$-Q2 scheme, the kinetic energy trends are similar to those observed with KEEP-Q2. However, due to the change in the internal energy numerical flux compared to KEEP-Q2, the entropy conservation error of KEEP$_{\text{PE}}$-Q2 increases to order 10^{-3} for $M_0 = 0.4$, whereas it remains comparable to that of KEEP-Q2 for $M_0 = 0.05$. Consequently, at $M_0 = 0.4$, we observe a mild growth in fluctuations for KEEP$_{\text{PE}}$-Q2 relative to KEEP-Q2, particularly in temperature, which increases linearly over time. Nevertheless, the KEEP$_{\text{PE}}$-Q2 scheme still achieves good entropy conservation compared to other schemes and maintains stable simulations with small thermodynamic fluctuations and no tendency to diverge.

The KEEP$_{\text{PE}}$-R-RA scheme also demonstrates excellent performance in preserving both kinetic energy and entropy, and in maintaining numerical stability. Its kinetic energy trends are similar to KEEP-Q2 and KEEP$_{\text{PE}}$-Q2. The entropy conservation error is an order of magnitude smaller than that of KEEP-Q2 for $M_0 = 0.05$, while for $M_0 = 0.4$, it remains comparable. The thermodynamic fluctuations also asymptotically reach a steady level close to that of KEEP-Q2.

The KGP-Q2, KEEP-Q2, KEEP$_{\text{PE}}$-Q2, and KEEP$_{\text{PE}}$-R-RA schemes accurately conserve the total mass, momentum (only the x-directional momentum is shown), total energy, and species mass up to machines precision for both $M_0 = 0.05$ and 0.4. Furthermore, there are almost no fluctuations in the species mass fraction for all non-diverging schemes, indicating that the mass fraction distributions remain uniform for $M_0 = 0.05$ and 0.4. This property is related to the numerical scheme applied to the species mass term and is further discussed in the next section.

In summary, the simulations presented in Section 4.1 indicate that both KEEP$_{\text{PE}}$-Q2 and KEEP$_{\text{PE}}$-R-RA schemes produce reliable results, with KEEP$_{\text{PE}}$-R-RA showing relative advantages, such as improved numerical stability in the 1D cases and better entropy conservation. Although the PE-F scheme provides superior PEP properties, it can introduce relatively large errors in density and entropy conservation in flows with less resolved mixture molar mass. Consequently, in the subsequent discussion of numerical schemes for the species equation, KEEP$_{\text{PE}}$ and KEEP$_{\text{PE}}$-R are used to discretise the continuity, momentum, and energy equations. PE-F is included as a comparison.

Furthermore, the results presented above imply a trade-off between maintaining global entropy conservation and preserving pressure equilibrium. To enforce both properties, a promising approach may be to employ a time-varying convex combination of KEEP-Q2 and KEEP$_{\text{PE}}$-Q2 following the adaptive weighting procedure proposed by Coppola et al. [21]. Incorporating the PE-F scheme could further allow the design of weighting parameters that minimise pressure-equilibrium errors in multi-component flows while retaining entropy conservation. These ideas are left for future work.

4.2. Species equation

In this section, to demonstrate the capability of the species mass numerical fluxes in maintaining the physical properties, including species mass conservation, uniform species mass fraction and temperature-equilibrium preservation, and to highlight the importance of using physically consistent species numerical fluxes, we examine the split forms listed in Section 3.4.2 in 1D advection problems and a 3D two-species, compressible Taylor–Green vortex flow. The properties in Table 2 are discussed. The list includes a group of species schemes, including DIV, KG, KGP, Q1, Q2, and Q3, using KEEP$_{\text{PE}}$ to discretise the continuity, momentum, and energy equations, and a second group, i.e., RA and RG, using KEEP$_{\text{PE}}$-R. Each test is labelled by the full combination of schemes used (e.g., KEEP$_{\text{PE}}$-Q2). Furthermore, PE-F is included in the TGV case (Section 4.2.3) for comparison but omitted from the 1D cases, where it reduces to KEEP$_{\text{PE}}$-Q2 under uniform species mass fractions (Section 4.2.1) or uniform mixture molar concentration (Section 4.2.2).

4.2.1. Uniform species mass fraction preservation: 1D advection

It has been demonstrated analytically in Section 3.3.3 that for flows with initially uniform species mass fractions, this uniformity should be preserved in time. Numerical schemes of the species convective term are required to be consistent with the schemes of the continuity equation (i.e., satisfying the condition outlined in Eq. (77)), to maintain this uniformity discretely, particularly under conditions with non-uniform density and velocity. In this section, we design a 1D advection problem with initially uniform species mass fractions but non-uniform density and velocity to validate the previous analysis and evaluate the schemes. We hereafter refer to this case as case S1. The initial conditions for case S1 are given as

$$u = 1 + 0.1\sin(2\pi x),\ p = 10,\ \rho = 2 + \sin(2\pi x),$$
$$Y_{\text{H}_2} = 0.5,\ Y_{\text{N}_2} = 1 - Y_{\text{H}_2},$$

where the velocity is a sinusoidal wave with a mean value of 1, the density follows the same sinusoidal distribution as the case by Shima et al. [31], and the pressure is increased to provide a smaller Mach number. There are two species in the mixture, H_2 and N_2,

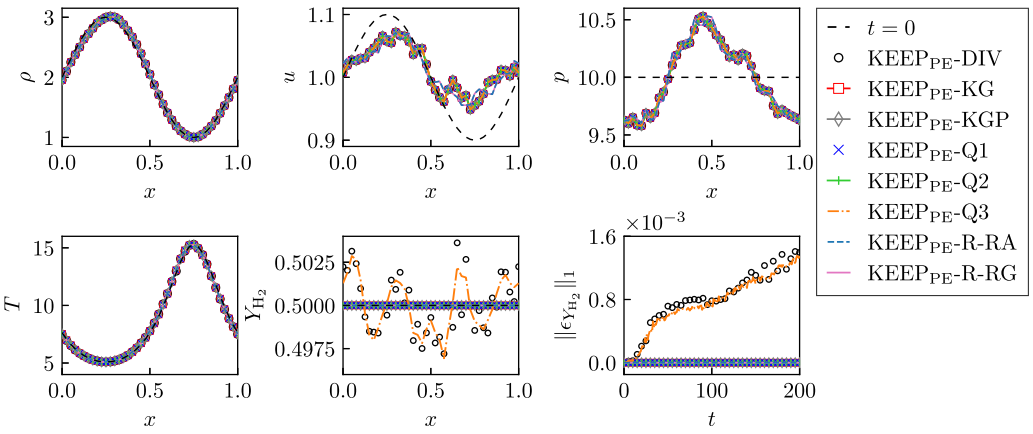

Fig. 7. The profiles for case S1: spatial distributions of density, velocity, pressure, temperature, and H_2 mass fraction at $t = 200$, and temporal evolution of H_2 mass fraction error.

with the same specific heat ratios, $\gamma_{H_2} = \gamma_{N_2} = 1.4$, and uniform distributions. The domain spans $0 \le x \le 1$ and the grid spacing is $\Delta x = 0.025$, uniform over the domain. The number of grid points is 41.

Fig. 7 shows the spatial distributions of ρ, u, p, T, and Y_{H_2} at $t = 200$. The last plot shows the temporal evolution of the L^1 norm of the Y_{H_2} error, $\|\epsilon_{Y_{H_2}}\|_1$. Since this is a nonlinear case, we see large variations in velocity and pressure. The mean velocity deviates from 1, causing phase errors in density and temperature waves. In terms of the Y_{H_2} profile, oscillations appear for computations using the KEEP$_{PE}$-DIV and KEEP$_{PE}$-Q3 schemes and increase with time, with the L^1-norm error reaching 1.6×10^{-3} at $t = 200$. The KEEP$_{PE}$-KG scheme produces marginal errors with the largest deviation in order 10^{-13} (not shown in the figure), whereas other schemes maintain the uniformity of species mass fraction up to machine precision.

This finding verifies the analytical deduction for Theorem 2, where it was pointed out that the form of the species numerical flux should be consistent with the form of the total mass numerical flux, to preserve mass fraction uniformity. The total mass numerical flux for the KEEP$_{PE}$ scheme (Eq. (43)) is in the quadratic-split form which separates the density and velocity; however, the DIV and Q3 forms reconstruct the density and velocity together, which does not satisfy the consistency condition (Eq. (77)) and hence sparks oscillations in the mass fraction. In contrast, the KGP, Q1, and Q2 forms reconstruct the density and velocity separately, therefore, preserving the uniformity. By assigning the species mass fractions as constants, the KG form reduces to a split form identical to that of the total mass, and consequently, maintains the uniformity, despite not being cast in a numerical flux. Similarly, the total mass numerical flux for KEEP$_{PE}$-R (Eq. (47)) separates the density and velocity while applying the square root of the density. Under uniform mass fraction, both RA and RG construct the density and velocity consistently with the total mass numerical flux, ensuring the uniformity of the species mass fraction.

4.2.2. *Temperature-equilibrium preservation: 1D advection*

In Section 3.3.3, we highlighted that for flows with initially uniform temperature, the equilibrium should be preserved in time, assuming the pressure and velocity are initially uniform and in equilibrium. To maintain this property discretely, particularly under conditions with non-uniform density and species mass fraction, the numerical flux of species mass should reconstruct the density and mass fraction together (i.e., satisfying the condition outlined in Eq. (97)). In this section, we design a 1D advection problem to demonstrate the analysis and evaluate the effect of species schemes on maintaining the temperature equilibrium. We hereafter refer to this case as case S2. The initial conditions for case S2 are given as

$$u = 1,\ p = 1,\ \rho = 2 + \sin(2\pi x),\ T = 1,$$
$$Y_{O_2} = 0.1,\ Y_{H_2} = f(p, \rho, T, Y_{O_2}),\ Y_{N_2} = 1 - Y_{H_2} - Y_{O_2},$$

where the temperature is set to unity, and the velocity, pressure, and density conditions follow the case by Shima et al. [31]. It is a three-species system composed of H_2, O_2, and N_2, with the same specific heat ratios, $\gamma_{H_2} = \gamma_{O_2} = \gamma_{N_2} = 1.4$. The initial H_2 mass fraction is $Y_{H_2} = f(p, \rho, T, Y_{O_2})$, denoting it is computed from these known variables using Eqs. (12) and (9). The density and H_2 mass fraction are set to vary over the domain, in order to expose the issue caused by inconsistent schemes. The O_2 mass fraction is initialised with a uniform profile; the reason why we add it is to explore the uniform mass fraction preservation capability of the schemes under a different initial condition from case S1. The domain spans $0 \le x \le 1$ and the grid spacing is $\Delta x = 0.025$, uniform over the domain. The total number of grid points is 41.

Fig. 8 presents the spatial distributions at $t = 200$ of ρ, p, Y_{H_2}, T, and Y_{O_2}, and the temporal evolution of the L^1-norm error for Y_{H_2}, T, c_{O_2}, and c_{H_2}. The schemes preserve the pressure (and velocity) equilibrium with minor errors of order 10^{-13}, attributed to the KEEP$_{PE}$ and KEEP$_{PE}$-R schemes (see case G1). Looking at the temperature profile, we find that oscillations appear in computations using the KG, KGP, Q1, and Q3 species forms with KEEP$_{PE}$, and both the RA and RG forms with KEEP$_{PE}$-R. These oscillations grow approximately linearly with time, reaching a maximum of around 0.002 at $t = 200$ for the KEEP$_{PE}$ group, but with smaller amplitudes

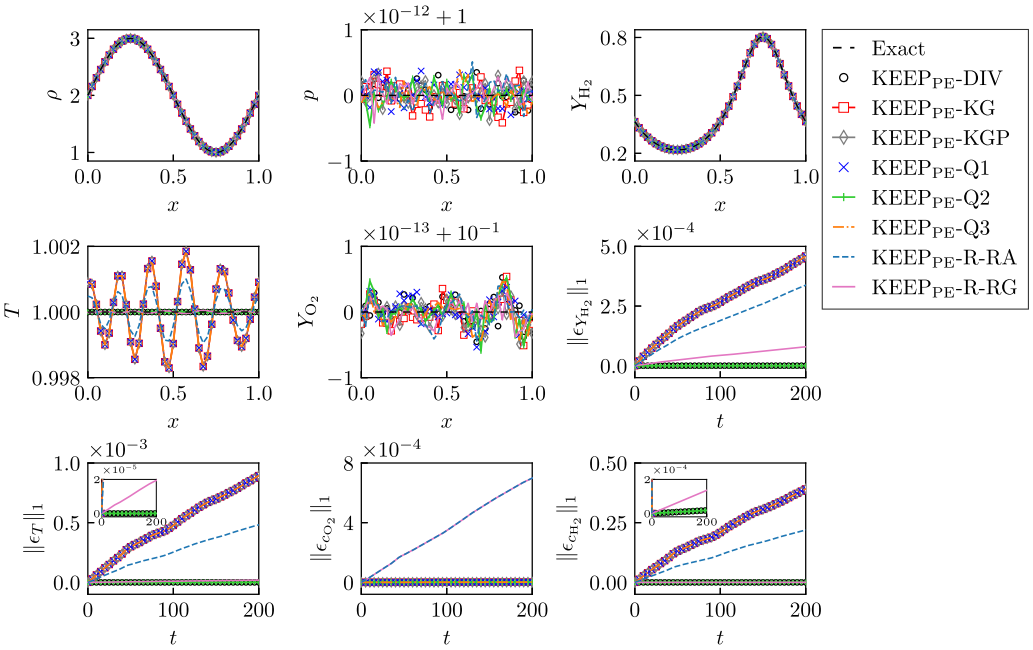

Fig. 8. The profiles for case S2: spatial distributions of density, pressure, H_2 mass fraction, temperature, and O_2 mass fraction at $t = 200$, and temporal evolution of errors in H_2 mass fraction, temperature, O_2 molar concentration, and H_2 molar concentration.

for the KEEP$_{PE}$-R group: about 0.001 with RA and only 5×10^{-5} with RG. The tendency of oscillations is nearly identical across the schemes (except for KEEP$_{PE}$-R-RG), suggesting that the underlying reason could be the same for them. On the contrary, the results show that KEEP$_{PE}$-DIV and KEEP$_{PE}$-Q2 maintain the temperature equilibrium, with marginal errors in order 10^{-13} (not shown in the figure).

The observations align with Theorem 3, which highlights that the ability of the species split form to constitute c_α at the discrete level is the key to preserving the temperature equilibrium. The DIV and Q2 species forms achieve this by reconstructing density and species mass fraction together at every grid point. In contrast, the KG, KGP, Q1, Q3, and RA species schemes, which reconstruct density and species mass fraction separately, cannot constitute c_α at every grid point, leading to errors in c_α and temperature. The RG species form is a special case – although it forms c_α at the discrete level, this structure does not hold for species N_s due to the nonlinear geometric means. As a result, the computation with RG produces temperature errors, but these errors are significantly smaller than those with RA, which fails to maintain the c_α structure for all species.

The temperature errors in computations using KG, KGP, Q1, Q3, RA, and RG species forms mainly arise from errors in the H_2 and N_2 molar concentrations. However, for species O_2, the initially uniform mass fraction of O_2 allows all species split forms to constitute c_{O_2} at every grid point, regardless of whether density and O_2 mass fraction are reconstructed together or separately. Consequently, all schemes yield only minor errors in the O_2 molar concentration, which are comparable within their respective groups (DIV, KG, KGP, Q1, Q2, and Q3 with KEEP$_{PE}$; RA and RG with KEEP$_{PE}$-R). Note that the difference between the two groups is caused by the different density means employed in each.

The errors in species molar concentrations also affect species mass fractions. For species H_2, increasing errors in Y_{H_2} are observed in simulations using the KG, KGP, Q1, Q3, RA, and RG species forms, exhibiting trends similar to the errors in c_{H_2}. This correlation stems from the relation $\partial Y_{H_2}/\partial t = (\partial \rho Y_{H_2}/\partial t - Y_{H_2}\partial \rho/\partial t)/\rho$, which indicates that inaccuracies in Y_{H_2} may arise from errors in the directly solved variables c_{H_2} (or ρY_{H_2}) and ρ. Given the relatively minor errors in ρ, the primary source of the observed errors in Y_{H_2} is likely c_{H_2}, explaining the similar error trends for Y_{H_2} and c_{H_2}. In contrast, KEEP$_{PE}$-DIV and KEEP$_{PE}$-Q2, which yield nearly zero errors in c_{H_2}, maintain Y_{H_2} errors close to zero. However, for species O_2, since all schemes achieve nearly the same accuracy for c_{O_2} within their respective groups, their solutions for Y_{O_2} are also nearly identical. Unlike in case S1, all schemes, including KEEP$_{PE}$-DIV and KEEP$_{PE}$-Q3, preserve the uniformity of Y_{O_2} in this case, with a minor error of order 10^{-14}. This is attributed to the initially uniform velocity profile in the current case, under which all species schemes remain consistent with their respective total mass numerical fluxes.

4.2.3. Conservation and scalar fluctuation: Inviscid Taylor–Green vortex

In this section, aiming to examine the effect of species numerical flux formulations in under-resolved turbulence simulations and determine the most reliable scheme, we present simulations of a two-species inviscid Taylor–Green vortex flow. The initial conditions

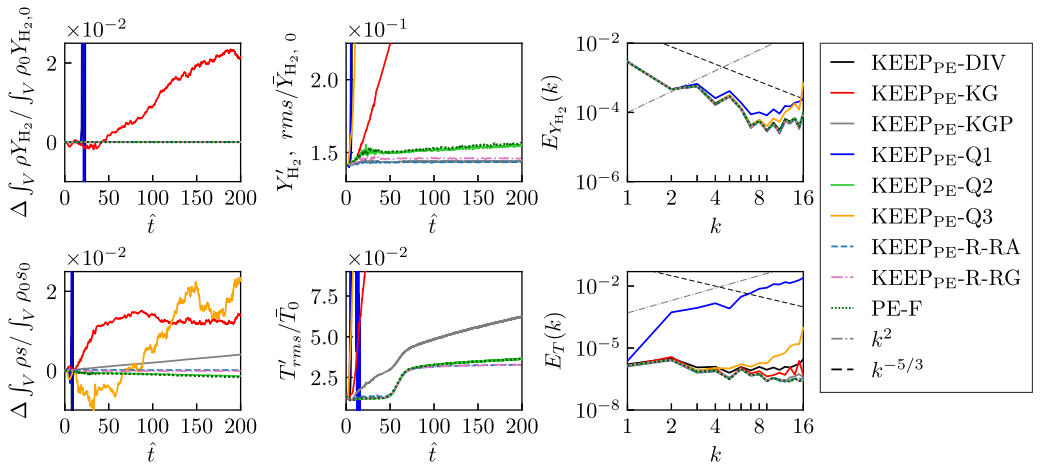

Fig. 9. Temporal evolution of H_2 mass, entropy, and rms fluctuations in H_2 mass fraction and temperature. Energy spectrum of three-dimensional H_2 mass fraction and temperature fields at $\hat{t} = 5$, for two-species inviscid TGV flow at $M_0 = 0.4$.

are adapted from the previous section by setting spatially varying density and mass fractions in the x direction:

$$
\begin{aligned}
Y_{H_2} &= 0.5 + 0.1\sin(x - \pi),\\
Y_{N_2} &= 1 - Y_{H_2},\\
\rho &= \rho_{sf,H_2} Y_{H_2} + \rho_{sf,N_2} Y_{N_2},\\
u &= M_0 \sin(x)\cos(y)\cos(z),\\
v &= -M_0 \cos(x)\sin(y)\cos(z),\\
w &= 0,\\
p &= \frac{1}{\gamma_0} + \frac{\rho {M_0}^2}{16}\Big(\cos(2x) + \cos(2y)\Big)\Big(\cos(2z) + 2\Big),
\end{aligned}
$$

where $\rho_{sf,H_2} = 0.1$ and $\rho_{sf,N_2} = 1$ are density scaling factors, $\gamma_0 = \gamma_{H_2} = \gamma_{N_2} = 1.4$, and $M_0 = 0.4$. The computational domain is a triply periodic box of dimension $[0, 2\pi]^3$, discretised uniformly with 33^3 grid points. We run the simulations up to $\hat{t} = 200$.

Fig. 9 illustrates the temporal evolution of the H_2 species mass, entropy, and rms fluctuations in H_2 mass fraction and temperature in the first two columns, which are computed in the same way as the plots in Figs. 5 and 6. Energy spectrum of 3D H_2 mass fraction and temperature fields at $\hat{t} = 5$ is presented in the last column of Fig. 9.

We see significant differences between the split forms. We begin by examining the KEEP$_{PE}$ group. For KEEP$_{PE}$-DIV and KEEP$_{PE}$-Q1, the rms values of the Y_{H_2} fluctuations diverge within $\hat{t} = 10$, which leads to breakdown of the H_2 species mass conservation. Subsequently, the computations of temperature diverge, and the entropies are no longer conserved. For KEEP$_{PE}$-Q3, although the onset of spurious oscillations in Y_{H_2} happens at nearly the same stage as KEEP$_{PE}$-DIV and KEEP$_{PE}$-Q1, the growth is considerably slower compared to them, and the scaled rms value is bounded within 4.8 until $\hat{t} = 200$. Hence, the integrated species mass remains conserved at machine precision. Nevertheless, the errors in Y_{H_2} still lead to divergence in the temperature computation at $\hat{t} \approx 10$, and subsequently increase the error in entropy conservation to approximately 2×10^{-2}. In terms of the KEEP$_{PE}$-KG scheme, spurious oscillations in Y_{H_2} increase slower and the scaled rms value reduces to 0.6 at $\hat{t} = 200$, relative to KEEP$_{PE}$-Q3. However, as the KG species form does not conserve species mass, the integrated species mass exhibits conservative errors, reaching 2×10^{-2} at $\hat{t} = 200$. The temperature oscillations from KEEP$_{PE}$-KG are also lower, and the rms value diverges later at $\hat{t} \approx 60$, compared to KEEP$_{PE}$-Q3. Consequently, the entropy production from the KEEP$_{PE}$-KG scheme is slightly less than that from KEEP$_{PE}$-Q3. On the other hand, the KEEP$_{PE}$-KGP and KEEP$_{PE}$-Q2 schemes substantially reduce the Y_{H_2} and temperature fluctuations compared with other schemes. Strict species mass conservation is maintained at machine precision, and their entropy conservation errors are in the order of 10^{-3}, lower than other schemes.

In case S1, KEEP$_{PE}$-DIV and KEEP$_{PE}$-Q3 fail to preserve mass fraction uniformity, which is attributed to inconsistency between the species flux and the total mass flux. Hence, it is reasonable that they yield significant Y_{H_2} oscillations in the current case, subsequently causing large temperature fluctuations. However, the improvement from KEEP$_{PE}$-Q1 to KEEP$_{PE}$-KGP is unexpected, as both preserve the mass fraction uniformity in case S1. Their only difference lies in the species scheme: Q1 reconstructs u and Y_{H_2} together, while KGP does so separately. A possible reason could be that during turbulence development, the increased velocity variations may enhance nonlinear effects. Thus, reconstructing Y_{H_2} together with u as in Q1 may make the Y_{H_2} solution more susceptible to nonlinearities, compared to the separate reconstruction in KGP. This explanation might also account for the lower Y_{H_2} fluctuations with Q2 than with Q1, as Y_{H_2} and u are reconstructed separately in Q2. Additionally, the reduced temperature fluctuations with Q2 may further lower Y_{H_2} fluctuations, as suggested by the observations from case S2. This analysis is supported by the Y_{H_2} energy spectrum, which exhibits

larger aliasing error in KEEP$_{PE}$-Q1 than in KEEP$_{PE}$-KGP and KEEP$_{PE}$-Q2. The KEEP$_{PE}$-KG scheme also features smaller aliasing in the Y_{H_2} spectrum compared to KEEP$_{PE}$-Q1, likely answering why it produces smaller Y_{H_2} oscillations. Furthermore, the improvement from KEEP$_{PE}$-KG to KEEP$_{PE}$-KGP may be attributed to the strict species mass conservation with the KGP species form yet not with KG, given that both schemes have the same ability in terms of uniform mass fraction preservation and temperature-equilibrium preservation, and also produce similar aliasing errors.

Comparing KEEP$_{PE}$-KGP and KEEP$_{PE}$-Q2, we observe that the former introduces slightly lower Y_{H_2} fluctuations. Similar to the above explanation, this may be attributed to that the KGP species flux, reconstructing ρ and Y_{H_2} separately, diminishes the influence of nonlinearities that are enhanced by the increased density variations during turbulence development. In spite of this, the temperature oscillations in KEEP$_{PE}$-Q2 are less than half of those in KEEP$_{PE}$-KGP. This reduction benefits from the temperature-equilibrium preservation property of Q2, as demonstrated in case S2. Eventually, KEEP$_{PE}$-Q2 results in a smaller deviation in entropy conservation compared to KEEP$_{PE}$-KGP. Furthermore, the results of KEEP$_{PE}$-Q2 closely match those of PE-F, unlike in case G1 where the former was more accurate. This is due to the smaller variations in species mass fractions, and thus in mixture molar mass in this case, which reduce differences between the two schemes.

Regarding the group of KEEP$_{PE}$-R schemes, the RA and RG split forms demonstrate similar performance. They produce low Y_{H_2} fluctuations similar to KEEP$_{PE}$-KGP, attributed to the property of uniform mass fraction preservation. However, despite lacking the property of temperature-equilibrium preservation, KEEP$_{PE}$-R-RA and KEEP$_{PE}$-R-RG both yield temperature fluctuations slightly lower than KEEP$_{PE}$-Q2. This is due to the excellent entropy-conservation property of KEEP$_{PE}$-R, leading to entropy conservation errors in an order of magnitude smaller than the KEEP$_{PE}$ scheme.

To summarise the tests on the species schemes, the analytical deductions in Section 3.3.3 are verified, and among the proposed schemes, KEEP$_{PE}$-Q2, the Q2 species numerical flux with the KEEP$_{PE}$ scheme, is demonstrated to be the only one that exhibits all considered physical properties, i.e., preserving the mass fraction uniformity and the temperature equilibrium under relevant conditions, and conserving species mass. While we did not find a scheme that fully preserves the temperature equilibrium for KEEP$_{PE}$-R, the RG split form exhibits relatively smaller errors than RA. In the inviscid TGV flow, satisfying these physical properties overall improves the accuracy of solutions for species mass fraction and temperature, and also aids in the conservation of species mass and entropy, which highlights the importance of using physically consistent forms in turbulence simulations. The physically consistent Q2 scheme outperforms all other species schemes, and therefore we consider it to be the preferred choice for the KEEP$_{PE}$ scheme. Note that although KEEP$_{PE}$-Q2 yields slightly larger mass fraction oscillations than KEEP$_{PE}$-KGP in the TGV flow, it demonstrates superiority in reducing the temperature oscillations and preserving the entropy conservation. Its performance is also comparable to that of PE-F. The KEEP$_{PE}$-R scheme is superior in entropy conservation, which results in small temperature oscillations for both RA and RG species schemes. However, due to the practical limitation of RG with negative mass fractions, RA might be a more reliable choice. Finally, it should be noted that while our tests demonstrated strong numerical robustness without the need for numerical dissipation, incorporating it may still be necessary in some cases to suppress high-wavenumber modes and improve solution quality (e.g., Edoh et al. [62]).

5. Conclusion

In this work, we developed high-order, non-dissipative, accurate, stable and physically consistent finite-difference schemes for turbulent compressible multi-component flow simulations. We firstly analysed the properties and characteristics of kinetic-energy-preserving, entropy-preserving, and pressure-equilibrium-preserving schemes in conditions with varying specific heats, and examined their performance in numerical experiments, with a comparison to other schemes. Next, for the convective terms in the species mass fraction transport equation, we constructed a split-form numerical flux that consistently satisfies key physical properties, including species mass conservation, uniform mass fraction preservation, and temperature-equilibrium preservation, and demonstrated its properties and capability by analytical deductions and through numerical tests.

In the 1D scalar advection tests on the schemes for continuity, momentum, and energy equations, the multi-component versions of the KEEP$_{PE}$ scheme, the KEEP$_{PE}$-R scheme, and the non-split standard central-difference scheme (DIV), i.e., KEEP$_{PE}$-Q2, KEEP$_{PE}$-R-RA, and DIV-Q2, respectively, were able to preserve pressure equilibrium and numerical stability in the case with a uniform specific heat ratio. For the cases with varying specific heats, KEEP$_{PE}$-Q2 and KEEP$_{PE}$-R-RA exhibited improved performance in preserving pressure equilibrium and numerical stability compared to other schemes that are not pressure-equilibrium-preserving by design, particularly for the case with a smooth sinusoidal $1/(\gamma - 1)$. Nevertheless, neither scheme guaranteed the pressure equilibrium and stability in a long-term run. Conversely, the PE-F scheme, designed for calorically perfect, multi-component flows, maintained the pressure equilibrium regardless of the γ distribution and exhibited better stability than KEEP$_{PE}$-Q2 and KEEP$_{PE}$-R-RA under varying specific heats. However, for the flows with less resolved mixture molar mass, PE-F led to errors in density and entropy conservation that negatively affected numerical stability. The tests on 3D inviscid TGV flows demonstrated that both KEEP$_{PE}$-Q2 and KEEP$_{PE}$-R-RA provided reliable results, with the latter showing relative advantages, particularly in entropy conservation. Both schemes outperform the scheme designed to reduce aliasing errors and the schemes that preserve merely kinetic energy or entropy, or neither.

For the species mass numerical flux, analytical deductions and 1D advection tests suggest that consistent reconstructions of density and velocity with the total mass numerical flux are necessary for preserving uniform mass fractions, and reconstructing density and mass fraction together is essential for preserving temperature equilibrium, under relevant conditions. The Q2 species formulation with the KEEP$_{PE}$ scheme (KEEP$_{PE}$-Q2) is the only form that satisfies both conditions and thereby maintains both uniform mass fraction preservation and temperature-equilibrium preservation properties. Due to the numerical flux formulation, Q2 also inherently maintains species mass conservation. In the 3D TGV test, the schemes designed to preserve uniform mass fractions mostly led to

lower mass fraction and temperature fluctuations, and the schemes designed to preserve temperature equilibrium usually resulted in smaller temperature fluctuations and entropy conservation errors. Strict species mass conservation also tended to help improve the overall accuracy. However, these outcomes may be influenced by nonlinearities of velocity, density, and mass fractions. While no scheme fully preserves the temperature equilibrium for KEEP_{PE}-R, the RG split form, using the geometric mean of partial densities, exhibits relatively smaller errors than RA, using the arithmetic mean of mass fractions. Due to the superiority of KEEP_{PE}-R in entropy conservation, using both RG and RA produces small temperature oscillations in the TGV test. However, due to the practical limitation of RG with negative mass fractions, RA may be a more reliable choice. For KEEP_{PE}, despite Q2 showing slightly higher mass fraction fluctuations than the cubic-split form, it exhibited superiority in reducing temperature oscillations and entropy conservation errors, with performance comparable to that of PE-F. Hence, we conclude that the Q2 form is the most reliable choice. The improved performance observed with Q2 highlights the importance of a species mass convective scheme being able to consistently preserve the key physical properties, including species mass conservation, uniform mass fraction preservation, and temperature-equilibrium preservation.

The physically consistent split-form framework provides an effective strategy for improving numerical stability and accuracy in simulations of compressible multi-component flows. Future work will explore adaptive blending procedures using time-varying convex combinations of schemes such as KEEP-Q2, KEEP_{PE}-Q2, and PE-F, to balance entropy conservation and pressure-equilibrium preservation (e.g., Coppola et al. [21]). Additional investigations will consider alternative formulations based on the multi-component PE-F scheme. Furthermore, the correction procedures of Abgrall [63] (see also Refs. [64–66]) offer an alternative to split forms for enforcing secondary physical consistencies and improving stability, which may also be worth exploring in future developments.

CRediT authorship contribution statement

Ye Wang: Writing – review & editing, Writing – original draft, Visualization, Software, Methodology, Formal analysis, Conceptualization; **Armin Wehrfritz:** Writing – review & editing, Supervision, Methodology, Conceptualization; **Evatt R. Hawkes:** Writing – review & editing, Supervision, Resources, Project administration, Funding acquisition.

Data availability

Data will be made available on request.

Declaration of competing interest

The authors declare that they have no known competing financial interests or personal relationships that could have appeared to influence the work reported in this paper.

Acknowledgements

This work was supported by the Australian Government through the Australian Research Council's Discovery Projects funding scheme (project DP200103535). A pool of computational resources was provided by the Australian Government through the Pawsey Supercomputing Centre and the National Computational Infrastructure under the National Computational Merit Allocation Scheme, and by the University of New South Wales.

Appendix A. The Proof of Theorem 1

Proof. Multiplying the semi-discrete continuity equation (Eq. (14)) by $(-u_i^2/2)|_m$ and the semi-discrete momentum (Eq. (15)) by $u_i|_m$, and adding them, we obtain the semi-discrete representation of the kinetic energy equation at grid point m:

$$\left.\frac{\partial \rho \frac{u_i^2}{2}}{\partial t}\right|_m + u_i|_m \frac{\hat{M}_{ij}|_{m+\frac{1}{2}} - \hat{M}_{ij}|_{m-\frac{1}{2}}}{\Delta x_j} - \frac{u_i^2}{2}|_m \frac{\hat{C}_j|_{m+\frac{1}{2}} - \hat{C}_j|_{m-\frac{1}{2}}}{\Delta x_j} + u_j|_m \frac{\hat{G}|_{m+\frac{1}{2}} - \hat{G}|_{m-\frac{1}{2}}}{\Delta x_j} = 0. \tag{A.1}$$

Multiplying Eq. (A.1) by the volume element $\Delta V = \Delta x \Delta y \Delta z$ (assuming uniform grid sizes in all directions) and summing over the grid points, we obtain the discrete volume integral of kinetic energy:

$$\sum_V \Delta V \left.\frac{\partial \rho \frac{u_i^2}{2}}{\partial t}\right|_m = \sum_x \sum_y \sum_z \left(- u_i|_m \frac{\hat{M}_{ij}|_{m+\frac{1}{2}} - \hat{M}_{ij}|_{m-\frac{1}{2}}}{\Delta x_j} + \frac{u_i^2}{2}|_m \frac{\hat{C}_j|_{m+\frac{1}{2}} - \hat{C}_j|_{m-\frac{1}{2}}}{\Delta x_j} - u_j|_m \frac{\hat{G}|_{m+\frac{1}{2}} - \hat{G}|_{m-\frac{1}{2}}}{\Delta x_j} \right) \Delta x \Delta y \Delta z. \tag{A.2}$$

We can organise Eq. (A.2) as:

$$\sum_V \Delta V \left.\frac{\partial \rho \frac{u_i^2}{2}}{\partial t}\right|_m = \sum_y \sum_z \mathcal{F}_x|_m \Delta y \Delta z + \sum_x \sum_z \mathcal{F}_y|_m \Delta x \Delta z + \sum_x \sum_y \mathcal{F}_z|_m \Delta x \Delta y, \tag{A.3}$$

where, for the j^{th} direction,

$$\mathcal{F}_j|_m = \sum_{x_j}\left(-u_i|_m\left(\hat{M}_{ij}|_{m+\frac{1}{2}} - \hat{M}_{ij}|_{m-\frac{1}{2}}\right) + \frac{u_i^2}{2}|_m\left(\hat{C}_j|_{m+\frac{1}{2}} - \hat{C}_j|_{m-\frac{1}{2}}\right) - u_j|_m\left(\hat{G}|_{m+\frac{1}{2}} - \hat{G}|_{m-\frac{1}{2}}\right)\right). \tag{A.4}$$

By assuming the grid points in the j^{th} direction are $[1\,..\,N]$ and using summation by parts, Eq. (A.4) is transformed into

$$\begin{aligned}\mathcal{F}_j|_m = &\sum_{m=1}^{N-1}\left(\hat{M}_{ij}|_{m+\frac{1}{2}}\left(u_i|_{m+1} - u_i|_m\right) - \hat{C}_j|_{m+\frac{1}{2}}\left(u_i|_{m+1} - u_i|_m\right)\frac{\left(u_i|_{m+1} + u_i|_m\right)}{2}\right) - u_i|_N\hat{M}_{ij}|_{N+\frac{1}{2}} + \frac{u_i^2}{2}|_N\hat{C}_j|_{N+\frac{1}{2}} + u_i|_1\hat{M}_{ij}|_{\frac{1}{2}} \\ &- \frac{u_i^2}{2}|_1\hat{C}_j|_{\frac{1}{2}} + \sum_{m=1}^{N-1}\hat{G}|_{m+\frac{1}{2}}\left(u_j|_{m+1} - u_j|_m\right) - u_j|_N\hat{G}|_{N+\frac{1}{2}} + u_j|_1\hat{G}|_{\frac{1}{2}}.\end{aligned} \tag{A.5}$$

By substituting for $\hat{C}_j$ and $\hat{M}_{ij}$ using Eqs. (40) and (41), respectively, and applying the proposed KEP condition (Eq. (42)), the right-hand-side first summation operator in Eq. (A.5) becomes

$$\begin{aligned}&\sum_{m=1}^{N-1}\left(\hat{M}_{ij}|_{m+\frac{1}{2}}\left(u_i|_{m+1} - u_i|_m\right) - \hat{C}_j|_{m+\frac{1}{2}}\left(u_i|_{m+1} - u_i|_m\right)\frac{\left(u_i|_{m+1} + u_i|_m\right)}{2}\right) = \sum_{l=1}^{L}a_{L,l}\sum_{m=1}^{N-1}\left(\sum_{k=0}^{l-1}\widetilde{(\rho,u_j,1)}_{m-k,l}\left(u_i|_{m-k+l} - u_i|_{m+1}\right)\right. \\ &\left. - \sum_{k=0}^{l-1}\widetilde{(\rho,u_j,1)}_{m-k,l}\left(u_i|_m - u_i|_{m-k}\right)\right)\left(u_i|_{m+1} - u_i|_m\right).\end{aligned} \tag{A.6}$$

By expanding terms $(u_i|_{m-k+l} - u_i|_{m+1})$ and $(u_i|_m - u_i|_{m-k})$, and changing the orders of summation, the two innermost summation operators can be converted to

$$\begin{aligned}&\sum_{k=0}^{l-1}\widetilde{(\rho,u_j,1)}_{m-k,l}\left(u_i|_{m-k+l} - u_i|_{m+1}\right) \\ &= \sum_{k=0}^{l-1}\widetilde{(\rho,u_j,1)}_{m-k,l}\left(\left(u_i|_{m-k+l} - u_i|_{m-k+l-1}\right) + \left(u_i|_{m-k+l-1} - u_i|_{m-k+l-2}\right) + \cdots + \left(u_i|_{m+3} - u_i|_{m+2}\right) + \left(u_i|_{m+2} - u_i|_{m+1}\right)\right) \\ &= \sum_{k=0}^{l-1}\sum_{q=1}^{l-1-k}\widetilde{(\rho,u_j,1)}_{m-k,l}\left(u_i|_{m+q+1} - u_i|_{m+q}\right) \\ &= \sum_{k=0}^{l-2}\sum_{q=1}^{l-1-k}\widetilde{(\rho,u_j,1)}_{m-k,l}\left(u_i|_{m+q+1} - u_i|_{m+q}\right),\end{aligned} \tag{A.7}$$

and,

$$\begin{aligned}&\sum_{k=0}^{l-1}\widetilde{(\rho,u_j,1)}_{m-k,l}\left(u_i|_m - u_i|_{m-k}\right) \\ &= \sum_{k=0}^{l-1}\widetilde{(\rho,u_j,1)}_{m-k,l}\left(\left(u_i|_{m-k+1} - u_i|_{m-k}\right) + \left(u_i|_{m-k+2} - u_i|_{m-k+1}\right) + \cdots + \left(u_i|_{m-1} - u_i|_{m-2}\right) + \left(u_i|_m - u_i|_{m-1}\right)\right) \\ &= \sum_{k=0}^{l-1}\sum_{q=1}^{k}\widetilde{(\rho,u_j,1)}_{m-k,l}\left(u_i|_{m-q+1} - u_i|_{m-q}\right) \\ &= \sum_{k=0}^{l-2}\sum_{q=1}^{l-1-k}\widetilde{(\rho,u_j,1)}_{m-q-k,l}\left(u_i|_{m-q+1} - u_i|_{m-q}\right),\end{aligned} \tag{A.8}$$

respectively, with which, Eq. (A.6) reduces to a formulation with only boundary terms, as:

$$\begin{aligned}&\sum_{m=1}^{N-1}\left(\hat{M}_{ij}|_{m+\frac{1}{2}}\left(u_i|_{m+1} - u_i|_m\right) - \hat{C}_j|_{m+\frac{1}{2}}\left(u_i|_{m+1} - u_i|_m\right)\frac{\left(u_i|_{m+1} + u_i|_m\right)}{2}\right) \\ &= \sum_{l=1}^{L}a_{L,l}\sum_{k=0}^{l-2}\sum_{q=1}^{l-1-k}\sum_{m=1}^{N-1}\left(\widetilde{(\rho,u_j,1)}_{m-k,l}\left(u_i|_{m+q+1} - u_i|_{m+q}\right)\left(u_i|_{m+1} - u_i|_m\right) - \widetilde{(\rho,u_j,1)}_{m-k-q,l}\left(u_i|_{m+1} - u_i|_m\right)\left(u_i|_{m+1-q} - u_i|_{m-q}\right)\right) \\ &= \sum_{l=1}^{L}a_{L,l}\sum_{k=0}^{l-2}\sum_{q=1}^{l-1-k}\sum_{p=0}^{q-1}\left(\widetilde{(\rho,u_j,1)}_{N-1-p-k,l}\left(u_i|_{N-p+q} - u_i|_{N-p+q-1}\right)\left(u_i|_{N-p} - u_i|_{N-p-1}\right)\right. \\ &\quad \left. - \widetilde{(\rho,u_j,1)}_{-p-k,l}\left(u_i|_{-p+q+1} - u_i|_{-p+q}\right)\left(u_i|_{-p+1} - u_i|_{-p}\right)\right) \\ &= \sum_{l=1}^{L}a_{L,l}\sum_{k=0}^{l-2}\sum_{q=1}^{l-1-k}\sum_{p=0}^{q-1}\left(\Phi|_N - \Phi|_1\right),\end{aligned} \tag{A.9}$$

where $\Phi|_m = \widetilde{(\rho, u_j, 1)}_{m-1-p-k,l}(u_i|_{m-p+q} - u_i|_{m-p+q-1})(u_i|_{m-p} - u_i|_{m-p-1})$. Plugging Eq. (A.9) into Eq. (A.5), we obtain

$$\mathcal{F}_j|_m = B.T. + P.T., \tag{A.10}$$

where $B.T.$ represents the boundary terms and $P.T.$ is the term of pressure work. For all directions $j = 1, 2, 3$, putting Eq. (A.10) into Eq. (A.3), i.e., summing Eq. (A.10) over the surface normal to direction j, demonstrates that the discrete volume integral of kinetic energy only consists of terms related to boundary and pressure work. □

Appendix B. Velocity equilibrium of the KEP schemes

Invoking the semi-discrete equations for total mass (Eq. (14)) and momentum (Eq. (15)), we substitute $\hat{C}_j$ with the generic formulation (Eq. (40)) in Theorem 1, substitute $\hat{M}_{ij}$ with the generic formulation (Eq. (41)) and the KEP condition (Eq. (42)) in Theorem 1, and substitute $\hat{G}$ with Eq. (56). Accordingly, we obtain:

$$\Delta x_j \left.\frac{\partial \rho}{\partial t}\right|_m = -2 \sum_{l=1}^{L} a_{L,l} \sum_{k=0}^{l-1} \left(\widetilde{(\rho, u_j, 1)}_{m-k,l} - \widetilde{(\rho, u_j, 1)}_{m-1-k,l} \right), \tag{B.1}$$

$$\begin{aligned} \Delta x_j \left.\frac{\partial \rho u_i}{\partial t}\right|_m = -2 \sum_{l=1}^{L} a_{L,l} \sum_{k=0}^{l-1} \Bigg(& \widetilde{(\rho, u_j, 1)}_{m-k,l} \frac{u_i|_{m-k} + u_i|_{m-k+l}}{2} - \widetilde{(\rho, u_j, 1)}_{m-1-k,l} \frac{u_i|_{m-1-k} + u_i|_{m-1-k+l}}{2} \\ & - \frac{p|_{m-k} + p|_{m-k+l} - p|_{m-1-k} - p|_{m-1-k+l}}{2} \Bigg). \end{aligned} \tag{B.2}$$

At time step t_n, assuming $u_i|_m^{t_n} = u_{i0}$ and $p|_m^{t_n} = p_0$, $\forall m$, Eq. (B.2) becomes:

$$\Delta x_j \left.\frac{\partial \rho u_i}{\partial t}\right|_m^{t_n} = -2 u_{i0} \sum_{l=1}^{L} a_{L,l} \sum_{k=0}^{l-1} \left(\widetilde{(\rho, u_j, 1)}_{m-k,l} - \widetilde{(\rho, u_j, 1)}_{m-1-k,l} \right) \Bigg|^{t_n}. \tag{B.3}$$

Next, by applying the product rule to the temporal derivative in Eq. (B.3):

$$\left.\frac{\partial \rho u_i}{\partial t}\right|_m^{t_n} = u_{i0} \left.\frac{\partial \rho}{\partial t}\right|_m^{t_n} + \rho|_m^{t_n} \left.\frac{\partial u_i}{\partial t}\right|_m^{t_n}, \tag{B.4}$$

then multiplying Eq. (B.1) by u_{i0} and subtracting it from Eq. (B.3), we derive:

$$\left.\frac{\partial u_i}{\partial t}\right|_m^{t_n} = 0, \ \forall m, \tag{B.5}$$

which indicates the velocity equilibrium is preserved over time.

Appendix C. Time-step convergence study on Taylor–Green vortex cases

To ensure the results and discussion of the Taylor–Green vortex tests are not influenced by time integration errors, we carried out a temporal convergence study using four different time steps corresponding to Courant numbers of approximately 0.5, 0.1, 0.05, and 0.02. We employed the classical four-stage fourth-order Runge–Kutta time integration and the eighth-order explicit central approximation, using the KEEP_{PE} scheme for continuity, momentum, and energy equations, and the Q2 scheme for the species equation.

Fig. C.10 shows the temporal evolution of kinetic energy, entropy, and rms temperature fluctuations for the Taylor–Green vortex cases in Section 4.1.2. At $M_0 = 0.05$, all time steps yield similar results. However, at $M_0 = 0.4$, differences between time steps are distinct. Reducing the Courant number from 0.5 to 0.05 alters the kinetic energy, entropy and temperature fluctuations, indicating that the results are affected by temporal errors. Further reducing the Courant number to 0.02 produces overlapping profiles with 0.05, suggesting that 0.05 is sufficiently small to achieve temporally converged results. The TGV case in Section 4.2.3 shows similar temporal convergence to the case here at $M_0 = 0.4$; thus, the results are not shown. Therefore, we confirm that a Courant number of 0.05 provides sufficiently small time steps to prevent temporal errors from affecting the results.

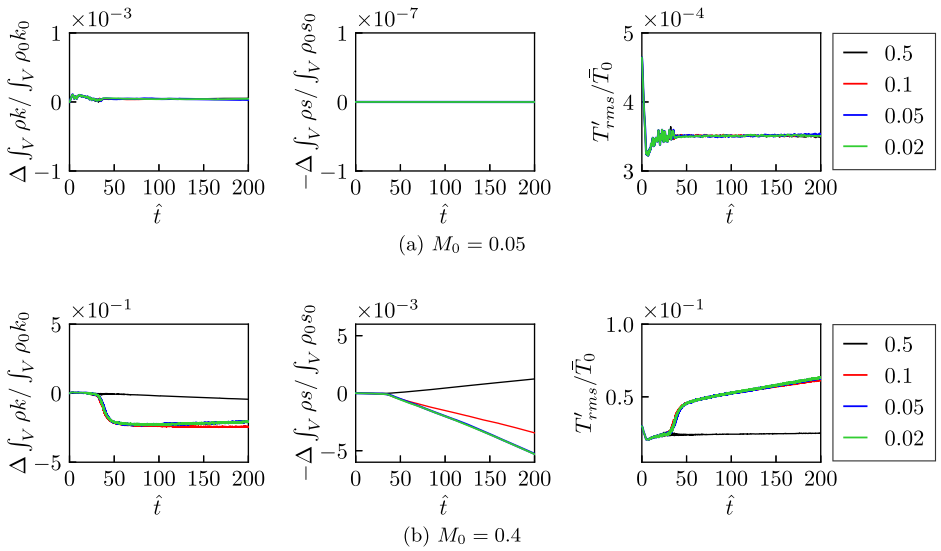

Fig. C.10. Temporal evolution of kinetic energy, entropy, and rms temperature fluctuations at different time steps, corresponding to Courant numbers of approximately 0.5, 0.1, 0.05, and 0.02, for the Taylor–Green vortex cases in Section 4.1.2 at (a) $M_0 = 0.05$ and (b) $M_0 = 0.4$.

References

[1] Y. Morinishi, Skew-symmetric form of convective terms and fully conservative finite difference schemes for variable density low-Mach number flows, J. Comput. Phys. 229 (2) (2010) 276–300. https://doi.org/10.1016/j.jcp.2009.09.021

[2] S. Pirozzoli, Generalized conservative approximations of split convective derivative operators, J. Comput. Phys. 229 (19) (2010) 7180–7190. https://doi.org/10.1016/j.jcp.2010.06.006

[3] J.C. Kok, A high-order low-dispersion symmetry-preserving finite-volume method for compressible flow on curvilinear grids, J. Comput. Phys. 228 (18) (2009) 6811–6832. https://doi.org/10.1016/j.jcp.2009.06.015

[4] G.J. Gassner, A.R. Winters, D.A. Kopriva, Split form nodal discontinuous Galerkin schemes with summation-by-parts property for the compressible Euler equations, J. Comput. Phys. 327 (2016) 39–66. https://doi.org/10.1016/j.jcp.2016.09.013

[5] S. Ghosal, An analysis of numerical errors in large-eddy simulations of turbulence, J. Comput. Phys. 125 (1) (1996) 187–206. https://doi.org/10.1006/jcph.1996.0088

[6] A.G. Kravchenko, P. Moin, On the effect of numerical errors in large eddy simulations of turbulent flows, J. Comput. Phys. 131 (1997) 310–322. https://doi.org/10.1006/jcph.1996.5597

[7] J. Larsson, S.K. Lele, P. Moin, Effect of numerical dissipation on the predicted spectra for compressible turbulence, Report, Center for Turbulence Research, 2007.

[8] C. Canuto, M.Y. Hussaini, A. Quarteroni, T.A. Zang, Spectral methods in fluid dynamics, Springer-Verlag, New York, 1988.

[9] C.A. Kennedy, A. Gruber, Reduced aliasing formulations of the convective terms within the Navier–Stokes equations for a compressible fluid, J. Comput. Phys. 227 (3) (2008) 1676–1700. https://doi.org/10.1016/j.jcp.2007.09.020

[10] S.K. Lele, Compact finite difference schemes with spectral-like resolution, J. Comput. Phys. 103 (1) (1992) 16–42. https://doi.org/10.1016/0021-9991(92)90324-R

[11] C.A. Kennedy, M.H. Carpenter, Several new numerical methods for compressible shear-layer simulations, Appl. Numer. Math. 14 (4) (1994) 397–433. https://doi.org/10.1016/0168-9274(94)00004-2

[12] A.K. Edoh, N.L. Mundis, C.L. Merkle, A.R. Karagozian, V. Sankaran, Comparison of artificial-dissipation and solution-filtering stabilization schemes for time-accurate simulations, J. Comput. Phys. 375 (2018) 1424–1450. https://doi.org/10.1016/j.jcp.2018.08.019

[13] G.A. Blaisdell, E.T. Spyropoulos, J.H. Qin, The effect of the formulation of nonlinear terms on aliasing errors in spectral methods, Appl. Numer. Math. 21 (3) (1996) 207–219. https://doi.org/10.1016/0168-9274(96)00005-0

[14] F. Ducros, F. Laporte, T. Soulères, V. Guinot, P. Moinat, B. Caruelle, High-order fluxes for conservative skew-symmetric-like schemes in structured meshes: application to compressible flows, J. Comput. Phys. 161 (1) (2000) 114–139. https://doi.org/10.1006/jcph.2000.6492

[15] Y. Kuya, S. Kawai, Modified wavenumber and aliasing errors of split convective forms for compressible flows, J. Comput. Phys. 464 (2022) 111336. https://doi.org/10.1016/j.jcp.2022.111336

[16] A.E. Honein, P. Moin, Higher entropy conservation and numerical stability of compressible turbulence simulations, J. Comput. Phys. 201 (2) (2004) 531–545. https://doi.org/10.1016/j.jcp.2004.06.006

[17] A. Jameson, Formulation of kinetic energy preserving conservative schemes for gas dynamics and direct numerical simulation of one-dimensional viscous compressible flow in a shock tube using entropy and kinetic energy preserving schemes, J. Sci. Comput. 34 (2) (2008) 188–208. https://doi.org/10.1007/s10915-007-9172-6

[18] Y. Morinishi, T.S. Lund, O.V. Vasilyev, P. Moin, Fully conservative higher order finite difference schemes for incompressible flow, J. Comput. Phys. 143 (1) (1998) 90–124. https://doi.org/10.1006/jcph.1998.5962

[19] W.J. Feiereisen, W.C. Reynolds, J.H. Ferziger, Numerical simulation of a compressible, homogeneous, turbulent shear flow. Report TF-13, thermosciences division, Mech. Eng. Stanford Univer. (1981) 759.

[20] P.K. Subbareddy, G.V. Candler, A fully discrete, kinetic energy consistent finite-volume scheme for compressible flows, J. Comput. Phys. 228 (5) (2009) 1347–1364. https://doi.org/10.1016/j.jcp.2008.10.026

[21] G. Coppola, F. Capuano, S. Pirozzoli, L. de Luca, Numerically stable formulations of convective terms for turbulent compressible flows, J. Comput. Phys. 382 (2019) 86–104. https://doi.org/10.1016/j.jcp.2019.01.007

[22] Y. Kuya, K. Totani, S. Kawai, Kinetic energy and entropy preserving schemes for compressible flows by split convective forms, J. Comput. Phys. 375 (2018) 823–853. https://doi.org/10.1016/j.jcp.2018.08.058

[23] W. Rozema, J.C. Kok, R.W.C.P. Verstappen, A.E.P. Veldman, A symmetry-preserving discretisation and regularisation model for compressible flow with application to turbulent channel flow, J. Turbul. 15 (6) (2014) 386–410. https://doi.org/10.1080/14685248.2014.910604

[24] A.K. Edoh, A new kinetic-energy-preserving method based on the convective rotational form, J. Comput. Phys. 454 (2022) 110971. https://doi.org/10.1016/j.jcp.2022.110971
[25] J. Nordström, A skew-symmetric energy and entropy stable formulation of the compressible Euler equations, J. Comput. Phys. 470 (2022) 111573. https://doi.org/10.1016/j.jcp.2022.111573
[26] A.E. Honein, Numerical aspects of compressible turbulence simulations, Thesis, 2005.
[27] E. Tadmor, The numerical viscosity of entropy stable schemes for systems of conservation laws. I, Math. Comput. 49 (179) (1987) 91–103. https://doi.org/10.2307/2008251
[28] P. Chandrashekar, Kinetic energy preserving and entropy stable finite volume schemes for compressible euler and Navier–Stokes Equations, J. Comput. Phys. 14 (5) (2013) 1252–1286. https://doi.org/10.4208/cicp.170712.010313a
[29] H. Ranocha, Generalised summation-by-parts operators and entropy stability of numerical methods for hyperbolic balance laws, Ph.D. thesis, Göttingen, 2018.
[30] S.S. Jain, P. Moin, A kinetic energy-and entropy-preserving scheme for compressible two-phase flows, J. Comput. Phys. 464 (2022) 111307. https://doi.org/10.1016/j.jcp.2022.111307
[31] N. Shima, Y. Kuya, Y. Tamaki, S. Kawai, Preventing spurious pressure oscillations in split convective form discretization for compressible flows, J. Comput. Phys. 427 (2021) 110060. https://doi.org/10.1016/j.jcp.2020.110060
[32] Y. Tamaki, Y. Kuya, S. Kawai, Comprehensive analysis of entropy conservation property of non-dissipative schemes for compressible flows: KEEP scheme redefined, J. Comput. Phys. 468 (2022) 111494. https://doi.org/10.1016/j.jcp.2022.111494
[33] H. Ranocha, G.J. Gassner, Preventing pressure oscillations does not fix local linear stability issues of entropy-based split-form high-order schemes, Commun. Appl. Math. Comput. (2021). https://doi.org/10.1007/s42967-021-00148-z
[34] C. De Michele, G. Coppola, Novel pressure-equilibrium and kinetic-energy preserving fluxes for compressible flows based on the harmonic mean, J. Comput. Phys. 518 (2024) 113338. https://doi.org/10.1016/j.jcp.2024.113338
[35] C. De Michele, G. Coppola, Asymptotically entropy-conservative and kinetic-energy preserving numerical fluxes for compressible Euler equations, J. Comput. Phys. 492 (2023) 112439. https://doi.org/10.1016/j.jcp.2023.112439
[36] S. Kawai, S. Kawai, Logarithmic mean approximation in improving entropy conservation in KEEP scheme with pressure equilibrium preservation property for compressible flows, J. Comput. Phys. 530 (2025) 113897. https://doi.org/10.1016/j.jcp.2025.113897
[37] R. Abgrall, How to prevent pressure oscillations in multicomponent flow calculations: a quasi conservative approach, J. Comput. Phys. 125 (1) (1996) 150–160. https://doi.org/10.1006/jcph.1996.0085
[38] R. Abgrall, S. Karni, Computations of compressible multifluids, J. Comput. Phys. 169 (2) (2001) 594–623. https://doi.org/10.1006/jcph.2000.6685
[39] G. Billet, R. Abgrall, An adaptive shock-capturing algorithm for solving unsteady reactive flows, Comput. Fluids 32 (10) (2003) 1473–1495. https://doi.org/10.1016/s0045-7930(03)00004-5
[40] E. Johnsen, F. Ham, Preventing numerical errors generated by interface-capturing schemes in compressible multi-material flows, J. Comput. Phys. 231 (17) (2012) 5705–5717. https://doi.org/10.1016/j.jcp.2012.04.048
[41] H. Terashima, S. Kawai, M. Koshi, Consistent numerical diffusion terms for simulating compressible multicomponent flows, Comput. Fluids 88 (2013) 484–495. https://doi.org/10.1016/j.compfluid.2013.10.007
[42] Y. Fujiwara, Y. Tamaki, S. Kawai, Fully conservative and pressure-equilibrium preserving scheme for compressible multi-component flows, J. Comput. Phys. 478 (2023) 111973. https://doi.org/10.1016/j.jcp.2023.111973
[43] E.J. Ching, R.F. Johnson, A.D. Kercher, Positivity-preserving and entropy-bounded discontinuous Galerkin method for the chemically reacting, compressible Euler equations. Part I: the one-dimensional case, J. Comput. Phys. 505 (2024) 112881. https://doi.org/10.1016/j.jcp.2024.112881
[44] A. Peyvan, K. Shukla, J. Chan, G. Karniadakis, High-order methods for hypersonic flows with strong shocks and real chemistry, J. Comput. Phys. 490 (2023) 112310. https://doi.org/10.1016/j.jcp.2023.112310
[45] M. Bernades, L. Jofre, F. Capuano, Kinetic-energy- and pressure-equilibrium-preserving schemes for real-gas turbulence in the transcritical regime, J. Comput. Phys. 493 (2023) 112477. https://doi.org/10.1016/j.jcp.2023.112477
[46] H. Terashima, N. Ly, M. Ihme, Approximately pressure-equilibrium-preserving scheme for fully conservative simulations of compressible multi-species and real-fluid interfacial flows, J. Comput. Phys. 524 (2025) 113701. https://doi.org/10.1016/j.jcp.2024.113701
[47] P. Trisjono, S. Kang, H. Pitsch, On a consistent high-order finite difference scheme with kinetic energy conservation for simulating turbulent reacting flows, J. Comput. Phys. 327 (2016) 612–628. https://doi.org/10.1016/j.jcp.2016.09.052
[48] P.K. Subbareddy, A. Kartha, G.V. Candler, Scalar conservation and boundedness in simulations of compressible flow, J. Comput. Phys. 348 (2017) 827–846. https://doi.org/10.1016/j.jcp.2017.08.001
[49] C. Pantano, R. Deiterding, D.J. Hill, D.I. Pullin, A low numerical dissipation patch-based adaptive mesh refinement method for large-eddy simulation of compressible flows, J. Comput. Phys. 221 (1) (2007) 63–87. https://doi.org/10.1016/j.jcp.2006.06.011
[50] B. Larrouturou, How to preserve the mass fractions positivity when computing compressible multi-component flows, J. Comput. Phys. 95 (1) (1991) 59–84. https://doi.org/10.1016/0021-9991(91)90253-H
[51] S. Kawai, S.K. Lele, Localized artificial diffusivity scheme for discontinuity capturing on curvilinear meshes, J. Comput. Phys. 227 (22) (2008) 9498–9526. https://doi.org/10.1016/j.jcp.2008.06.034
[52] J.H. Chen, A. Choudhary, B. de Supinski, M. DeVries, E.R. Hawkes, S. Klasky, W.K. Liao, K.L. Ma, J. Mellor-Crummey, N. Podhorszki, R. Sankaran, S. Shende, C.S. Yoo, Terascale direct numerical simulations of turbulent combustion using S3D, Comput. Sci. Discov. 2 (1) (2009) 015001. https://doi.org/10.1088/1749-4699/2/1/015001
[53] P.C. Ma, Y. Lv, M. Ihme, An entropy-stable hybrid scheme for simulations of transcritical real-fluid flows, J. Comput. Phys. 340 (2017) 330–357. https://doi.org/10.1016/j.jcp.2017.03.022
[54] O. Desjardins, G. Blanquart, G. Balarac, H. Pitsch, High order conservative finite difference scheme for variable density low Mach number turbulent flows, J. Comput. Phys. 227 (15) (2008) 7125–7159. https://doi.org/10.1016/j.jcp.2008.03.027
[55] P. Lax, B. Wendroff, Systems of conservation laws, Commun. Pure Appl. Math. 13 (2) (1960) 217–237. https://doi.org/10.1002/cpa.3160130205
[56] T.C. Fisher, M.H. Carpenter, J. Nordström, N.K. Yamaleev, C. Swanson, Discretely conservative finite-difference formulations for nonlinear conservation laws in split form: theory and boundary conditions, J. Comput. Phys. 234 (2013) 353–375. https://doi.org/10.1016/j.jcp.2012.09.026
[57] Y. Kuya, S. Kawai, High-order accurate kinetic-energy and entropy preserving (KEEP) schemes on curvilinear grids, J. Comput. Phys. 442 (2021) 110482. https://doi.org/10.1016/j.jcp.2021.110482
[58] Y. Kato, Y. Kuya, Secondary conservation properties of compact schemes in split forms, J. Comput. Phys. 528 (2025) 113829. https://doi.org/10.1016/j.jcp.2025.113829
[59] K. Koga, T. Kajishima, Low dissipative finite difference hybrid scheme by discontinuity sensor of detecting shock and material interface in multi-component compressible flows, J. Comput. Phys. 448 (2022). https://doi.org/10.1016/j.jcp.2021.110757
[60] A. Jameson, W. Schmidt, E. Turkel, Numerical solution of the Euler equations by finite volume methods using Runge Kutta time stepping schemes, in: 14th Fluid and Plasma Dynamics Conference, 1981, p. 1259. https://doi.org/10.2514/6.1981-1259
[61] F. Capuano, G. Coppola, L. Rández, L. de Luca, Explicit Runge–Kutta schemes for incompressible flow with improved energy-conservation properties, J. Comput. Phys. 328 (2017) 86–94. https://doi.org/10.1016/j.jcp.2016.10.040
[62] A.K. Edoh, N.L. Mundis, A.R. Karagozian, V. Sankaran, Balancing aspects of numerical dissipation, dispersion, and aliasing in time-accurate simulations, Int. J. Numer. Methods Fluids 92 (11) (2020) 1506–1527. https://doi.org/10.1002/fld.4837
[63] R. Abgrall, A general framework to construct schemes satisfying additional conservation relations. Application to entropy conservative and entropy dissipative schemes, J. Comput. Phys. 372 (2018) 640–666. https://doi.org/10.1016/j.jcp.2018.06.031
[64] R. Abgrall, P. Öffner, H. Ranocha, Reinterpretation and extension of entropy correction terms for residual distribution and discontinuous Galerkin schemes: application to structure preserving discretization, J. Comput. Phys. 453 (2022) 110955. https://doi.org/10.1016/j.jcp.2022.110955

[65] Y. Mantri, P. Öffner, M. Ricchiuto, Fully well-balanced entropy controlled discontinuous Galerkin spectral element method for shallow water flows: global flux quadrature and cell entropy correction, J. Comput. Phys. 498 (2024) 112673. https://doi.org/10.1016/j.jcp.2023.112673
[66] A.K. Edoh, Conservative correction procedures utilizing artificial dissipation operators, J. Comput. Phys. 504 (2024) 112880. https://doi.org/10.1016/j.jcp.2024.112880